*Human Molecular Genetics, 2013, Vol. 22, No. 17* **3460–3476**
*doi:10.1093/hmg/ddt201*
*Advance Access published on May 6, 2013*

# APP/PS1 mice overexpressing SREBP-2 exhibit combined Aβ accumulation and tau pathology underlying Alzheimer's disease

**Elisabet Barbero-Camps[1,2], Anna Fernández[1,2], Laura Martínez[1,2], Jose C. Fernández-Checa[1,2,3,*] and Anna Colell[1,2,*]**

[1]Department of Cell Death and Proliferation, IIBB-CSIC and [2]Liver Unit, Hospital Clinic, IDIBAPS and CIBEREHD, Barcelona 08036, Spain and [3]Southern California Research Center for ALPD and Cirrhosis, Keck School of Medicine of the University of Southern California, Los Angeles 90033, CA, USA

Received March 12, 2013; Revised April 30, 2013; Accepted April 30, 2013

**Current evidence indicates that excess brain cholesterol regulates amyloid-β (Aβ) deposition, which in turn can regulate cholesterol homeostasis. Moreover, Aβ neurotoxicity is potentiated, in part, by mitochondrial glutathione (mGSH) depletion. To better understand the relationship between alterations in cholesterol homeostasis and Alzheimer's disease (AD), we generated a triple transgenic mice featuring sterol regulatory element-binding protein-2 (SREBP-2) overexpression in combination with APPswe/PS1ΔE9 mutations (APP/PS1) to examine key biochemical and functional characteristics of AD. Unlike APP/PS1 mice, APP/PS1/SREBP-2 mice exhibited early mitochondrial cholesterol loading and mGSH depletion. Moreover, β-secretase activation and Aβ accumulation, correlating with oxidative damage and neuroinflammation, were accelerated in APP/PS1/SREBP-2 mice compared with APP/PS1 mice. Triple transgenic mice displayed increased synaptotoxicity reflected by loss of synaptophysin and neuronal death, resulting in early object-recognition memory impairment associated with deficits in spatial memory. Interestingly, tau pathology was present in APP/PS1/SREBP-2 mice, manifested by increased tau hyperphosphorylation and cleavage, activation of tau kinases and neurofibrillary tangle (NFT) formation without expression of mutated tau. Importantly, *in vivo* treatment with the cell permeable GSH ethyl ester, which restored mGSH levels in APP/PS1/SREBP-2 mice, partially prevented the activation of tau kinases, reduced abnormal tau aggregation and Aβ deposition, resulting in attenuated synaptic degeneration. Taken together, these results show that cholesterol-mediated mGSH depletion is a key event in AD progression, accelerating the onset of key neuropathological hallmarks of the disease. Thus, therapeutic approaches to recover mGSH may represent a relevant strategy in the treatment of AD.**

## INTRODUCTION

Cholesterol homeostasis is impaired in Alzheimer's disease (AD) brain. Accumulation of sterols has been described in senile plaques and in affected brain areas from AD patients and mouse models (1–5), with reported region-specific loss of synapses related to changes in cholesterol levels (6). Although several studies examining the effect of different lipid lowering compounds in AD have produced mixed outcomes, the epidemiological data linking high cholesterol levels with increased amyloid-β (Aβ) production and prevalence of AD are supported by a growing number of *in vivo* and *in vitro* studies (7). Accordingly, cholesterol enrichment in lipid rafts has been postulated to upregulate the activity of Aβ-synthesizing enzymes (8–10). Once generated, cholesterol levels can also influence the Aβ aggregation state (11) and the rate of degradation (12). In turn, Aβ has been described to modulate cholesterol homeostasis (1,13,14), establishing a self-sustained cycle between cholesterol accumulation and Aβ generation. In line with this vicious cycle, AD transgenic mice with acyl-CoA:cholesterolacyltransferases

*To whom correspondence should be addressed at: Department of Cell Death and Proliferation. Institut d'Investigacions Biomèdiques de Barcelona (IIBB-CSIC). Rosselló 161, Barcelona 08036, Spain. Tel: +34 933638300; Fax: +34 933638301; Email: anna.colell@iibb.csic.es (A.C.)/checa229@yahoo.com (J.C.F.-C.)

deletion exhibited a reduced sterol synthesis rate and improved amyloid pathology (15). Moreover, subcutaneous administration of β-cyclodextrin in Tg19959 mice significantly diminished Aβ deposition, tau phosphorylation and improved memory deficits (16), reinforcing the connection between altered cholesterol and AD pathology. Additionally, our previous studies have unraveled a new role of cholesterol in Aβ cytotoxicity, whereby mitochondrial cholesterol loading sensitized to Aβ neurotoxicity via mitochondrial glutathione (mGSH) depletion (5,17).

Although it is widely accepted that Aβ is an initial and important part in the pathogenesis of AD, additional factors such as abnormal tau phosphorylation associated with neurofibrillary tangle (NFT) formation are required for AD to progress from a presymptomatic state to the appearance of dementia symptoms (18). Interestingly, several lines of experimental evidence have shown that Aβ potentiates tau pathology, therefore positioning tau abnormalities downstream of Aβ in AD (19–21). It has been also suggested that hyperphosphorylation of tau may be attributable to mitochondrial oxidative stress (22). Furthermore, studies using *Drosophila* as a model system demonstrate that the loss of axonal mitochondria promotes tau phosphorylation and enhances tau-mediated neurodegeneration (23). The relationship between mitochondrial dysfunction and tau pathology is further supported by a recent work linking mitochondrial dynamics to tau toxicity in neurons (24).

Notably, it has been reported that tangle-bearing neurons contain increased levels of free cholesterol than adjacent tangle-free neurons (25). The presence of AD-type NFTs is also a distinctive feature of the hereditary neurodegenerative disorder Niemann-Pick type C disease (NPC) (26), characterized by a defect in cellular cholesterol trafficking that leads to accumulation of unesterified cholesterol and other lipids, in particular sphingolipids, in late endocytic organelles and mitochondria (5,27). Further studies in mouse models of NPC confirmed that cholesterol deregulation is a key pathogenic event affecting tau homeostasis in parallel with amyloid accumulation (28–30). Recently, the overexpression of APP in Npc1-deficient mice has been shown to accelerate the behavioral and neuropathological abnormalities characteristic of these mice, whereas treatment with β-cyclodextrin significantly reduces brain cholesterol levels, increases longevity and attenuates pathological markers, therefore defining a functional mechanism shared by AD and NPC, and regulated by cholesterol (31). Tau hyperphosphorylation has also been described in apolipoprotein E-deficient mice fed with a high cholesterol diet (32,33).

Unfortunately, it has been challenging to develop genetically engineered mouse models that recapitulate all of the neuropathological hallmarks of the disease. For example, unlike humans, the expression of amyloid precursor protein (APP) and presenilin (PS) mutant variants in mice has proved to be insufficient to promote NFTs and overt neurodegeneration (18,34). To overcome this limitation, mice harboring human tau mutations associated with frontotemporal dementia have been extensively used to study neurofibrillary pathology, despite the absence of linkage of these mutations to AD in humans. However, tau involved in NFT is invariably wild type (WT) in AD, and hence a trustable model of AD-like tau pathology remains still elusive.

Based on these data, it is likely that alterations in the intracellular cholesterol content could influence tau pathology by promoting tangle formation without the presence of pathogenic mutations in tau, and therefore accelerate AD-like pathology progression. To test this hypothesis, here we have generated APP/PS1 mice that constitutively overexpress the active truncated form of sterol regulatory element-binding protein-2 (SREBP-2). APP/PS1/SREBP-2 mice have increased brain cholesterol levels associated with a selective depletion of mGSH. Compared with APP/PS1 mice, triple transgenic mice display enhanced neuroinflammation, increased oxidative stress damage and neuronal death associated with cognitive decline. Several tau kinases are activated in these mice, leading to hyperphosphorylated tau and NFT formation. Moreover, *in vivo* treatment of APP/PS1/SREBP-2 mice with GSH ethyl ester, which restores the pool of mGSH and prevents oxidative stress, has a direct impact on tau pathology and amyloid plaques, and results in less synaptic degeneration. These data provide evidence for the relevance of preserving the mitochondrial antioxidant defence as a therapeutic strategy in AD.

## RESULTS

### Triple transgenic mice exhibit mitochondrial cholesterol loading and accelerated β-secretase activation and Aβ accumulation

To analyze how overexpression of SREBP-2 modulates the course of different AD-related pathological hallmarks triggered by brain accumulation of cholesterol, we generated a triple transgenic model harboring the human Swedish mutant APP(Swe), the human mutant PS1(ΔE9) and the human SREBP-2 transgenes. In line with previous observations in SREBP-2 mice (5), the triple transgenic mice displayed increased cholesterol levels, both in total brain extracts and in the mitochondrial fraction, associated with a selective depletion of mGSH levels at all the ages analyzed (Table 1), while the total GSH content in brain remained unaltered across all the genotypes (data not shown). Similar increases of cholesterol, either in total brain and in mitochondria, with the subsequent mGSH depletion was also noticed in 10-month-old APP/PS1 mice, consistent with previous findings, suggesting that Aβ metabolism regulates cholesterol homeostasis (1,13,14).

In accordance with the notion that cholesterol potentiates the amyloidogenic processing of APP and Aβ generation (9–11), 4-month-old APP/PS1/SREBP-2 mice exhibited increased β-secretase activity (Fig. 1A) and immunohistological staining of diffused Aβ depositions in hippocampus (Fig. 1B) as well as increased incidence of high human Aβ (1-42) levels (Fig. 1C), which further increased at 7 and 10 months of age. These changes, however, lagged behind in APP/PS1 mice being detectable at 7 months of age (Fig. 1A–C). Similar results were observed when the levels of endogenous Aβ were analyzed (Supplementary Material, Fig. S1). Importantly, no activation of β-secretase or high levels of Aβ was observed in SREBP-2 transgenic mice (Fig. 1A and Supplementary Material, Fig. S1), indicating that the elevation of brain cholesterol *per se* is not sufficient to trigger Aβ synthesis and accumulation.

### Exacerbated oxidative stress and neuroinflammation in APP/PS1/SREBP-2 mice

We next analyzed markers of oxidative stress. Protein oxidation was enhanced in APP/PS1/SREBP-2 mice, exhibiting an

**Table 1.** Increased cholesterol levels associated with mitochondrial GSH depletion in mice carrying the SREBP-2 transgene

| | WT | SREBP-2 | APP/PS1 | APP/PS1/SREBP-2 |
|---|---|---|---|---|
| Total cholesterol from brain homogenate and isolated mitochondria | | | | |
| Homogenate | | | | |
| 4-month | 113.7 ± 7.2 | 160.9 ± 20.4* | 103.6 ± 8.2 | 171.4 ± 17.7* |
| 7-month | 110.4 ± 11.4 | 144.5 ± 7.70* | 105.4 ± 9.1 | 166.3 ± 9.10* |
| 10-month | 113.6 ± 2.7 | 140.9 ± 13.6* | 170.9 ± 29.9* | 154.5 ± 23.6* |
| Mitochondria | | | | |
| 4-month | 5.67 ± 0.46 | 10.89 ± 1.82* | 5.22 ± 1.13 | 12.48 ± 3.18* |
| 7-month | 5.01 ± 1.67 | 10.82 ± 2.91* | 4.08 ± 1.13 | 11.98 ± 1.87* |
| 10-month | 4.86 ± 2.04 | 13.80 ± 0.59* | 15.29 ± 4.46* | 17.52 ± 2.01* |
| Mitochondrial GSH | | | | |
| 4-month | 3.58 ± 0.68 | 1.95 ± 0.16* | 3.67 ± 0.74 | 1.61 ± 0.19* |
| 7-month | 3.31 ± 0.30 | 1.93 ± 0.23* | 2.95 ± 0.32 | 1.70 ± 0.36* |
| 10-month | 3.44 ± 0.56 | 1.82 ± 0.38* | 1.77 ± 0.44* | 1.52 ± 0.58* |

*$P < 0.05$ versus WT values. ($n = 8$ per genotype). Values are expressed as mean ± SD; mean differences were compared by one-way ANOVA with Dunnett's *post hoc* test.

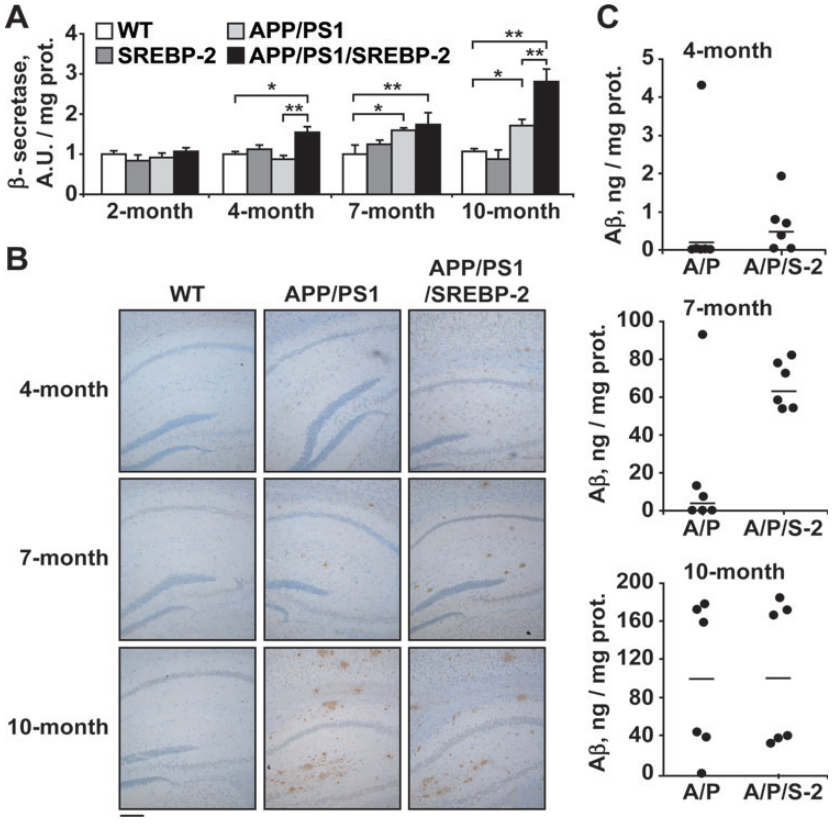


**Figure 1.** Increased cholesterol promotes Aβ synthesis and loading. (**A**) β-Secretase activity analyzed in brain extracts from WT and transgenic mice (AU: arbitrary units). *$P < 0.05$, **$P < 0.01$ ($n = 3$). Values are expressed as mean ± SD (**B**) Representative photomicrographs of hippocampus labeled with human anti-Aβ(1-42) and counterstained with hematoxylin showing early Aβ depositions in APP/PS1/SREBP-2 mice. Scale bar: 100 μm. (**C**) Brain from WT and indicated mutant mice (A/P: APP/PS1 mice; A/P/S-2: APP/PS1/SREBP-2 mice) were homogenized with guanidine HCl extraction buffer, and the homogenates were analyzed by ELISAs for quantitative assessment of the human Aβ(1-42) content at the indicated ages ($n = 6$ per genotype).

age-dependent increase of protein carbonyl groups analyzed either spectrophotometrically (Fig. 2A) and by western blot (Supplementary Material, Fig. S2). Overexpression of SREBP-2 in APP/PS1 mice also resulted in increased oxidative DNA damage determined by 8-hydroxyguanosine immunostaining of hippocampus from 7-month-old mice (Fig. 2B). Associated with the oxidative damage, we observed an age-dependent rise of the inflammatory cytokine interleukine-1 beta (IL-1β) in APP/PS1/SREBP-2 mice (Fig. 2C). The increment of IL-1β expression was also detectable in SREBP-2 and APP/PS1 mice at older ages (Fig. 2C). The accelerated neuroinflammation displayed by the triple transgenic mice was further

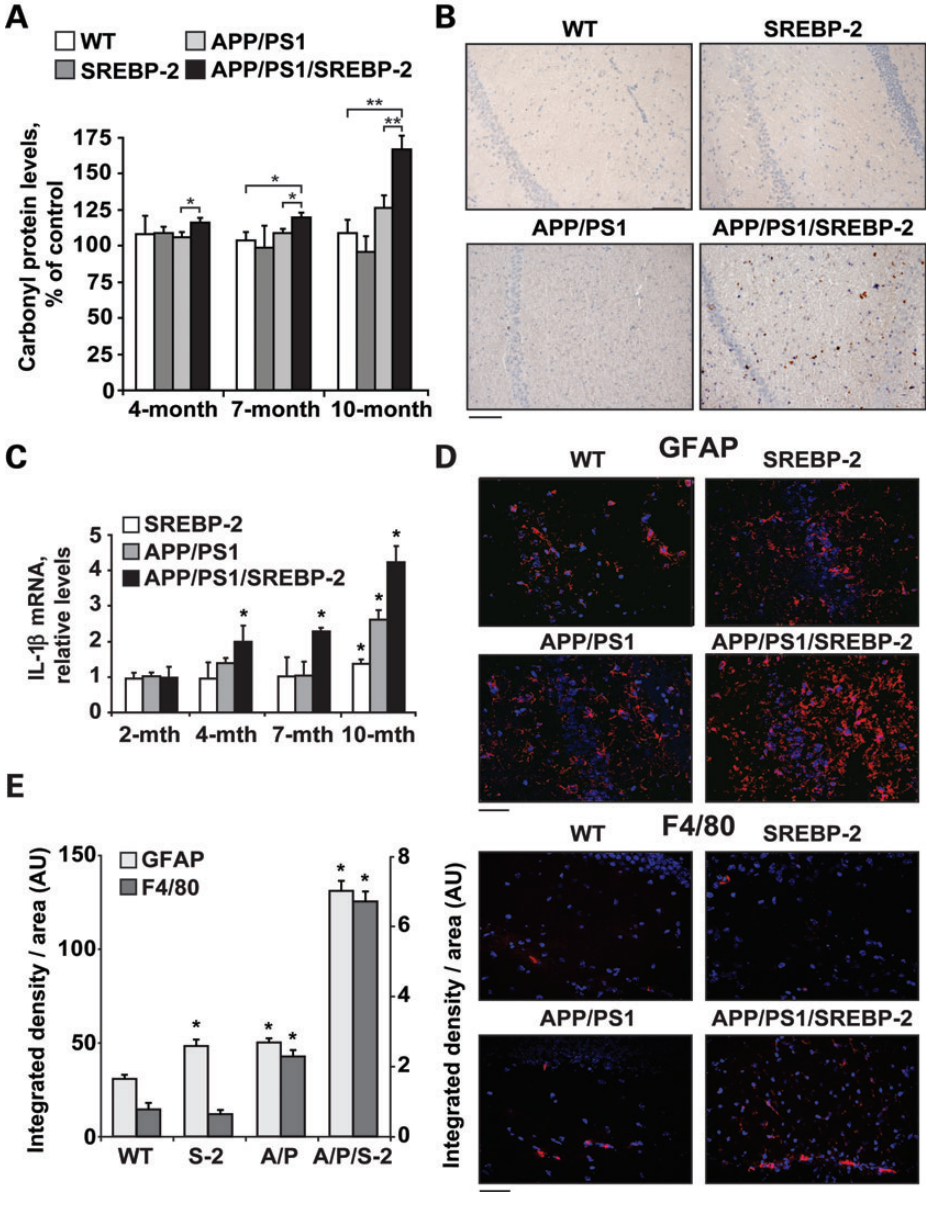


**Figure 2.** SREBP-2 overexpression in APP/PS1 mice exacerbates oxidative stress and neuroinflammation. (**A**) Protein carbonyl content from brain of the indicated genotype analyzed spectrophotometrically. $^{*}P < 0.05$, $^{**}P < 0.01$ ($n = 6$). (**B**) Immunohistochemical staining of 8-hydroxyguanosine (8-OHG). Representative photomicrographs of hippocampus showing nuclear presence of 8-OHG in 7-month-old APP/PS1-SREBP-2 mice, which is indicative of oxidative DNA damage. Scale bar: 100 μm. (**C**) mRNA levels of IL-1β in brain from the indicated genotype analyzed by a quantitative PCR. Absolute mRNA values were determined, normalized to 18S and reported as relative levels referred to the expression in WT mice. $^{*}P < 0.05$ versus WT values ($n = 6$). (**D** and **E**) Activation of astrocytes and microglia analyzed by GFAP and F4/80 immunostaining, respectively. (D) Representative confocal images of GFAP and F4/80 immunofluorescence (red) of hippocampal sections from 7- and 4-month-old mice, respectively. Nuclei were stained with Hoechst 33258 (blue). Scale bar: 50 μm. (E) Quantification of GFAP (left axis) and F4/80 (right axis) immunoreactivity by integrated density analysis. $^{*}P < 0.01$ ($n = 6$). Values are expressed as mean ± SD.

confirmed by immunohistochemical analysis of glial fibrillary acidic protein (GFAP) indicating enhanced astrogliosis in hippocampal samples from 7- and 10-month-old mice (Fig. 2D and Supplementary Material, Fig. S3). Microglial activation preceded astrogliosis in APP/PS1/SREBP-2 mice with increased presence of F4/80 positive cells already detectable at 4 month of age (Fig. 2D). Quantitation of the area occupied by the immunoreactive glial structures also revealed a significant gliosis in 7-month-old SREBP-2 and APP/PS1 mice but to a much lesser extent than in those of triple transgenic mice (Fig. 2E).

## Overexpression of SREBP-2 promotes synaptotoxicity and neuronal death in APP/PS1 mice

Despite the fact that neuronal loss is a key feature of human AD, cell death is limited in most mouse models of β-amyloidosis and become only evident in older specimens. Particularly, in APP/PS1 mice, the presence of apoptotic markers and hippocampal neuronal loss has been reported in brain sections from 16-month-old onwards (35,36). In contrast, our previous studies using mouse models of cholesterol loading described

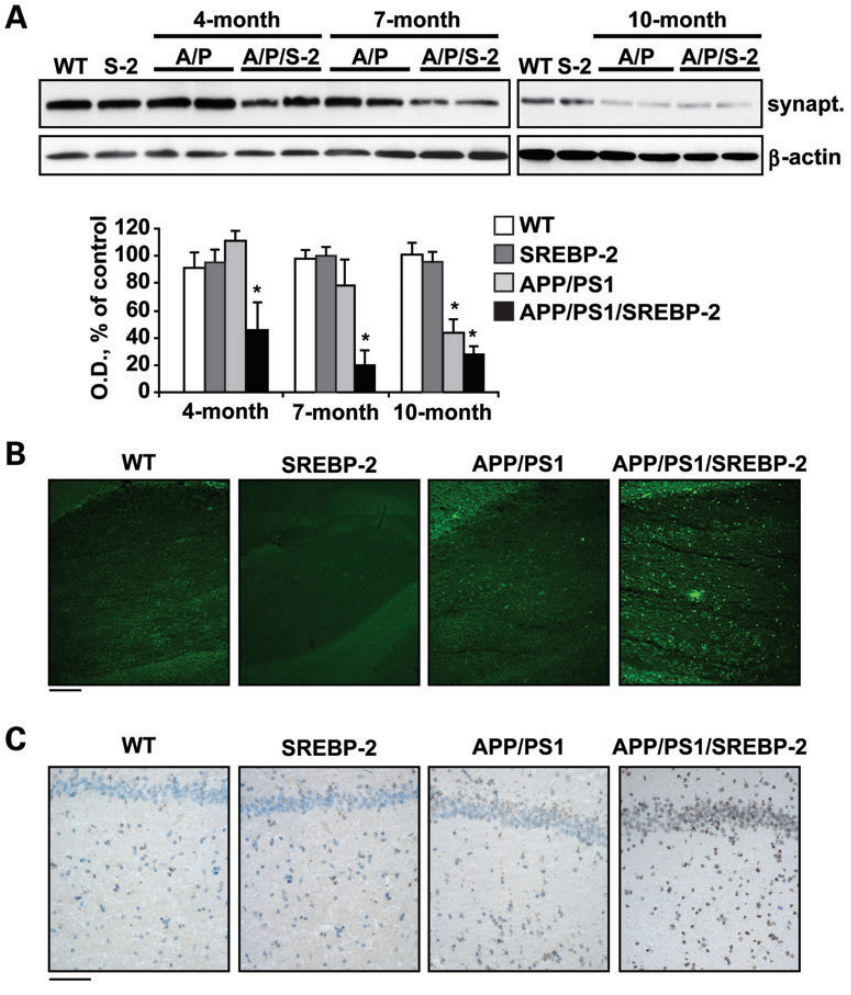


**Figure 3.** APP/PS1/SREBP-2 mice exhibit enhanced neuronal damage. (**A**) Representative immunoblotting showing synaptophysin (synapt.) protein levels from WT and indicated mutant mice (S-2: SREBP-2 mice; A/P: APP/PS1 mice; A/P/S-2: APP/PS1/SREBP-2 mice). Densitometric values of the bands representing synaptophysin immunoreactivity were normalized with the values of the corresponding β-actin bands (OD: normalized optical density). $^{*}P < 0.05$ versus WT values ($n = 3$). Values are expressed as mean ± SD. (**B**) Representative images of degenerated neurons in hippocampal regions from 10-month-old mice by Fluoro-Jade B staining. Scale bar: 100 μm. (**C**) Representative images of apoptotic cells in hippocampus from 10-month-old mice by a terminal deoxynucleotidyl transferase mediated nick-end labeling assay (TUNEL assay). Scale bar: 50 μm.

an age-independent and enhanced susceptibility to Aβ neurotoxicity, resulting from an accumulation of cholesterol in mitochondria that favored Aβ-induced cell death due to mGSH depletion (5). In line with these data, we observed that overexpression of SREBP-2 in APP/PS1 mice accelerated the decline of the presynaptic marker synaptophysin, starting at 4 months of age with further progression in 7- and 10-month-old mice (Fig. 3A), whereas this outcome was only significant in 10-month-old APP/PS1 mice (Fig. 3A). Moreover, the increased synaptic degeneration displayed by APP/PS1/SREBP-2 mice was accompanied with a marked neuronal death analyzed by Fluoro-Jade B staining (Fig. 3B) and TUNEL assay (Fig. 3C) in hippocampal CA1 regions of 10-month-old mice. In contrast, at this age signs of neuronal damage were almost negligible in APP/PS1 mice (Fig. 3B and C). Taken together, these observations emphasize the key role of cholesterol in regulating the neurodegenerative process.

### SREBP-2 overexpression in APP/PS1 mice impairs short-term recognition memory but does not worsen spatial memory deficits

To determine whether the increased neuronal damage observed in the triple transgenic mice can influence cognitive performance, we evaluated spatial memory acquisition and retention abilities in all four groups at 7 month of age. We first analyzed the performance of mice in a non-spatial cued platform variant of the Morris water maze (MWM). As seen, all the groups exhibited similar escape latencies to the visible platform indicating no differences in vision and motivation (Fig. 4A). When the spatial hippocampus-dependent MWM was tested, all mice exhibited similar escape latencies to the hidden platform (Fig. 4A), indicating that the learning kinetics during the acquisition phase were similar among the groups. Conversely, in the probe trial when the platform was removed, one-way ANOVA indicated

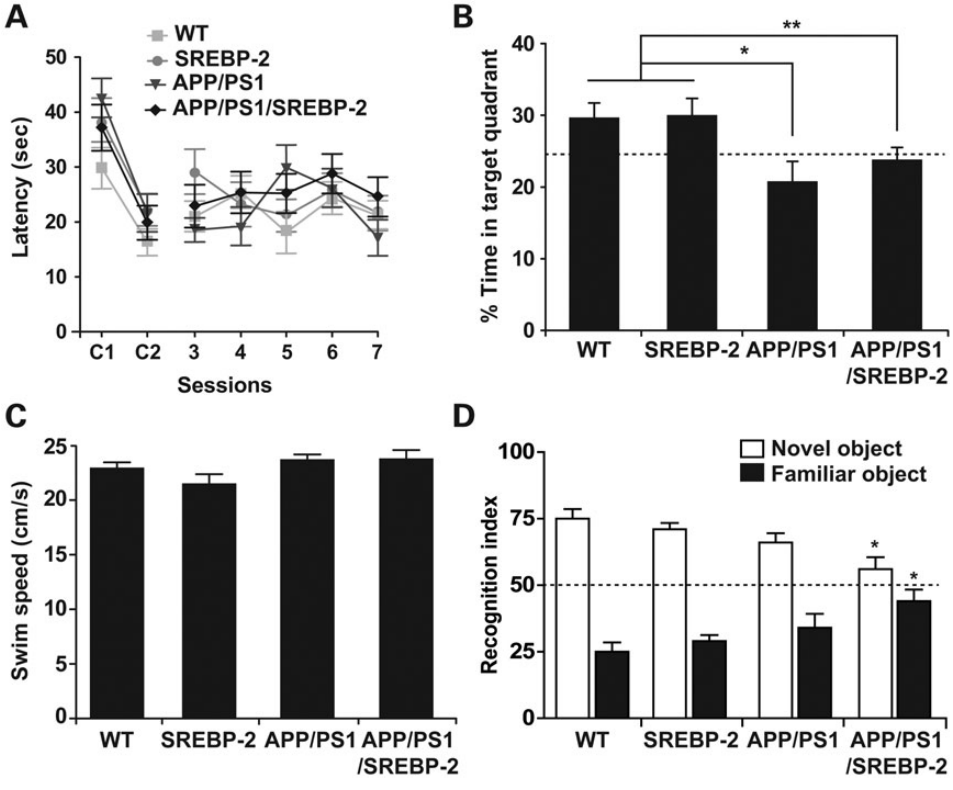


**Figure 4.** SREBP-2 overexpression in APP/PS1 mice does not worsen the spatial memory deficits but impairs short-term recognition memory. MWM was used to evaluate the spatial memory deficits in 7-month-old mice ($n = 10–15$ per genotype). (**A**) Cognitive performance in cued tasks (C1 and C2) and acquisition sessions (3–7) measured as mean time to locate the escape platform. All mouse strains showed similar latencies to reach the platform in the nonspatial variant of the MWM (C1 and C2). Learning rates during spatial memory acquisition were similar between groups. (**B**) Performance in the probe trial measured as mean percentage time spent in the target quadrant. APP/PS1 and APP/PS1/SREBP-2 mice showed no preference for the target quadrant relative to the other quadrants, whereas mice without APP/PS1 expression preferred the target quadrant. $^{*}P < 0.01$, $^{**}P < 0.05$. (**C**) Swimming speed exhibiting no significant differences among groups. (**D**) A novel object recognition test was used to assess deficits in short-term recognition memory in 7-month-old mice ($n = 7–12$ per genotype). Shown is the recognition index, which is the amount of time exploring the novel or familiar object versus the overall exploration time multiplied by 100. APP/PS1 mice that overexpress SREBP-2 exhibited a similar preference between novel and familiar objects. $^{*}P < 0.05$ versus WT values. Values are expressed as mean ± SD.

significant changes in the time the mice spent in the target quadrant, while WT and SREBP-2 transgenic mice preferred the target quadrant, APP/PS1 mice showed no preference for the target quadrant relative to the other three quadrants (Fig. 4B). The impaired memory retention displayed by the APP/PS1 mice was unaffected by SREBP-2 overexpression (Fig. 4B). These differences cannot be accounted for motor deficits, as the swim speeds across all four genotypes were equivalent (Fig. 4C). Mice were also tested using the object recognition paradigm, a behavioral task mainly dependent on cortical areas, including the perirhinal cortex (37,38). This test exploits the natural tendency of mice to explore objects perceived as novel. We found that whereas recognition memory in WT, SREBP-2 and APP/PS1 mice was intact (Fig. 4D), triple transgenic mice failed to discriminate between novel and familiar objects (Fig. 4D). The impairment in object recognition memory in addition to the spatial memory deficits displayed by APP/PS1/SREBP-2 mice may therefore reflect a wider brain area affected relative to that in APP/PS1 mice, implying that brain deterioration in triple transgenic mice expands to the perirhinal cortex in addition to hippocampus.

## SREBP-2 overexpression in APP/PS1 mice enhances the development of tau pathology

Abnormal tau hyperphosphorylation and aggregation are present in NPC (26) and treatment with the cholesterol-lowering drug 2-hydroxypropyl-β-cyclodextrin significantly attenuates the neurofibrillary pathology in NPC patients and animal models (31,39), therefore, suggesting a link between cholesterol and tauopathy. Based on these observations, we analyzed the phosphorylation status of tau in triple transgenic mice. In particular, we focused on phospho Ser-396 and phospho Ser-202/Thr-205 (AT8) residues, as these have been widely used for the detection of NFTs in AD. APP/PS1/SREBP-2 displayed an age-dependent increase in phospho Ser-396 starting at 4 month of age and high AT8 immunoreactivity detectable at 4 and 10 month of age (Fig. 5A), while tau phosphorylation (AT8 immunoreactivity) was significant in 10-month-old APP/PS1 mice (Fig. 5A). Levels of total tau (tau-5) were unchanged in all the groups and at all the ages analyzed (Fig. 5A). Since tau phosphorylation can result in disruption of microtubule stability and formation of insoluble tau aggregates, we evaluated the solubility of tau

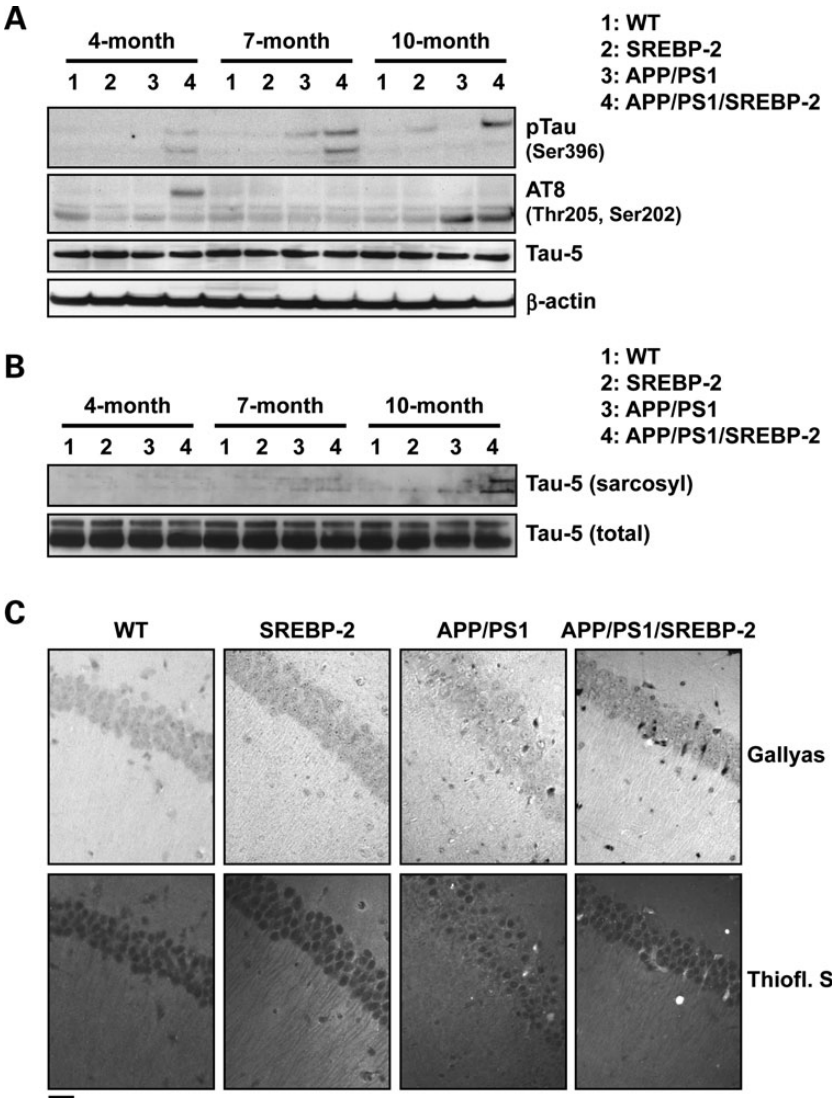


**Figure 5.** SREBP-2 overexpression in APP/PS1 mice enhances the development of neurofibrillary pathology. (**A**) Protein extracted from brain homogenates of WT and mutant mice at the indicated ages analyzed by western blot to assess phosphorylation levels of tau at different epitopes recognized by the indicated phosphorylation-dependent and site-specific anti-tau antibodies. Total tau levels were detected by the phosphorylation-independent antibody Tau-5. (**B**) Protein immunoblots showing total (non-phosphorylated and phosphorylated) tau (Tau-5) in crude and sarcosyl-insoluble fractions from brain homogenates of WT and mutant mice at the indicated ages. (**C**) Representative sections of hippocampus from 10-month-old mice showing increased Gallyas-stained NFTs and thioflavin-S-positive cells in APP/PS1/SREBP-2 mice. Scale bar: 50 μm.

by fractionation of crude extracts with sarkosyl. Western blot analyses revealed sarkosyl-insoluble tau accumulation exclusively in brain extracts from APP/PS1/SREBP-2 mice (Fig. 5B). To assess whether the insoluble tau content in triple transgenic mice undergoes structural changes resembling NFT, sections of hippocampus from 10-month-old mice were examined with Gallyas silver and thioflavin S stains (Fig. 5C). Significantly, APP/PS1/SREBP-2 mice showed an increased number of Gallyas-positive inclusions compared with APP/PS1 mice, which were also stained with the amyloid-specific dye thioflavin S (Fig. 5C). Additionally, we performed immunohistochemistry of hippocampal slices from 10-month-old APP/PS1/SREBP-2 mice, using the phospho-dependent anti-tau antibody AT8 in combination with different brain cell type-specific markers (Supplementary Material, Fig. S4). The confocal analyses confirmed that hyperphosphorylated tau specifically co-localized with the neuronal marker microtubule-associated protein 2 (MAP2), forming small aggregates mainly within the somatodendritic compartments. Although glial fibrillary tangles have been reported in AD (40), no co-localization was observed between AT8 and GFAP or myelin basic protein (MBP), therefore, discarding the presence of tau inclusions in astrocytes and oligodendrocytes (Supplementary Material, Fig. S4).

### APP/PS1/SREBP-2 mice exhibit activation of kinases involved in tau phosphorylation

We next analyzed the activity profile of various protein kinases implicated in tau phosphorylation, including glycogen synthase kinase-3 beta (GSK-3β), cyclin-dependent kinase 5 (CDK5) and the family members of mitogen-activated protein kinase (MAPK): extracellular signal-regulated kinase 1/2 (ERK 1/2),

stress-activated protein kinase/Jun-amino-terminal kinase (SAPK/JNK) and p38 MAPK. As an indication of the activity, we determined the ratio of the immunoreactivity of the active phosphorylated form and the total level of each kinase (Supplementary Material, Fig. S5). As seen, the three MAPK examined were activated in APP/PS1/SREBP-2 mice (Fig. 6A), with an early phosphorylation of p38 MAPK beginning at 4 months of age, followed by phosphorylation of SAPK/JNK and ERK 1/2 at the latter age. In contrast, APP/PS1 mice showed a significant activation of SAPK/JNK by 7 month of age (Fig. 6A). As for GSK-3β, both the active (phospho Tyr-216) and the inactive (phospho Ser-9) forms were investigated (Fig. 6B). APP/PS1/SREBP-2 mice showed an age-dependent increase of phosphorylated Tyr-216, starting at 7 months of age. Associated with this increase, we observed a reduction of the inhibitory Ser-9 phosphorylation, which was already evident in 4-month-old mice (Fig. 6B). In APP/PS1 mice levels of phosph Ser-9 decreased at 10 month of age but did not correlate with a significant increase in phospho Tyr-216. SREBP-2 overexpression in APP/PS1 mice also promoted the activation of CDK5 at all ages (Fig. 6C), reflected by phosphorylated CDK5 and increased conversion of p35 to p25, the neuronal activator of CDK5, in brain from 7- and 10-month-old APP/PS1/SREBP-2 mice. Total CDK5 levels were not significantly different between the four genotypes (Fig. 6C). Since it has been reported a connection between loss of function of protein phosphatase 2A (PP2A) and tau hyperphosphorylation (41) we checked the expression of the catalytic C subunit of the enzyme and the levels of phosphorylated PP2A C at Tyr307, which inhibits the enzyme activity (Fig. 6D). As seen, total levels of PP2A C subunit remained unaltered in the four groups and at all ages (Fig. 6D). Additionally, the degree of phosphorylation-dependent inhibition was similar between groups, with an age-dependent tendency to decrease in all genotypes. Taken together these observations provide evidence that cholesterol regulate tau phosphorylation by promoting the activation of several tau kinases and discard a contributory role of phosphatases in this event.

### Increased proteolytic cleavage of tau protein in mice harboring the SREBP-2 transgene

Toxic tau aggregation can be accelerated by proteolytic cleavage (42). Cleaved tau serves as a nucleation center for the pathological assembly of tau filaments. Consequently, cellular conditions that increase tau levels and fragmentation could favor formation of NFT. Since recent evidences suggested that cholesterol can indirectly promote tau fragmentation by modulating the activity of several proteases, including calpain and cathepsin D (31,43,44), we investigated the generation of cleaved tau fragments in the triple transgenic mice (Fig. 7A). Total levels of tau remained almost unchanged between all the genotypes; however, when films were over-exposed we observed the presence of cleaved tau fragments in APP/PS1/SERBP-2 mice by 4 month of age. Interestingly, despite absence of NFT (Fig. 5B and C), brain extracts from SREBP-2 mice also showed fragmented tau (Fig. 7A), suggesting that cleavage of tau triggered by cholesterol is not sufficient to promote tau aggregation and toxicity. Next, we checked cleavage of α-spectrin into calpain-specific signature fragments as a marker of calpain activity (Fig. 7B).

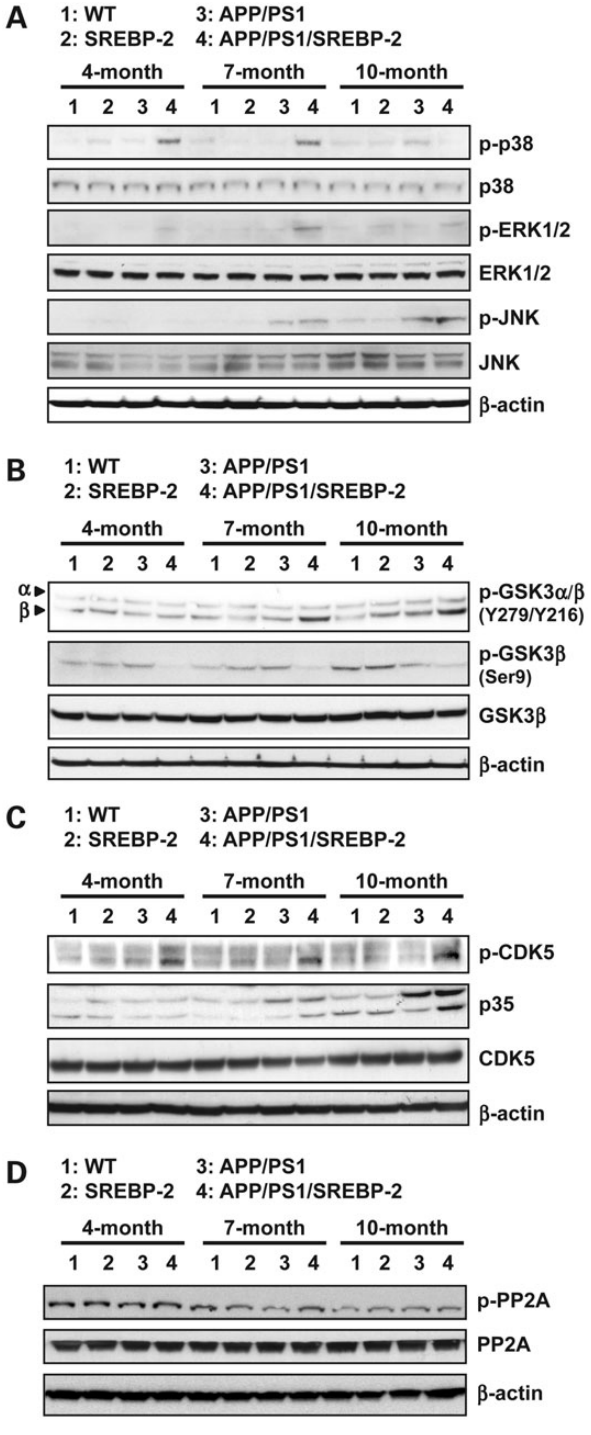


**Figure 6.** Activation profiles of different kinases associated with tau phosphorylation. (**A**) Representative immunoblots of cerebral homogenates from WT and indicated mutant mice using antibodies against the non-phosphorylated and active phosphorylated forms of ERK 1/2, JNK and p38 MAPK. As shown, all three MAPK pathways were activated in APP/PS1/SREBP-2 mice. (**B**) Western blot analysis of GSK-3β activation with antibodies against Y279 and Y216 (activating sites) and Ser9 (inhibitory site) indicating enhanced GSK-3β activity in APP/PS1 mice that overexpress SREBP-2. (**C**) Representative immunoblots showing increased levels of phosphorylated CDK5 and enhanced cleavage of p35 (CDK5 activator protein) at 10 months of age in brain extracts from APP/PS1/SREBP-2 mice. (**D**) Western blot analysis of PP2A activation using the PP2A C subunit antibody and the phospho-specific antibody that recognize the inhibitory phosphorylation at Tyr307 in subunit C.

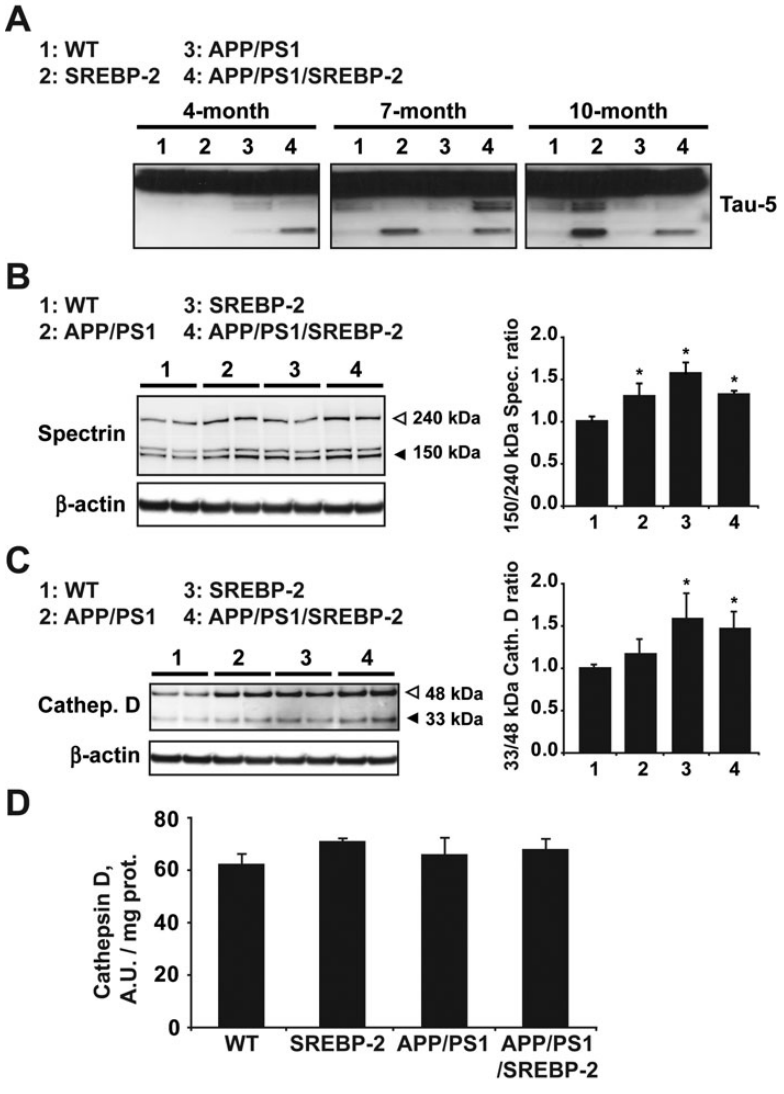


**Figure 7.** Increased proteolytic cleavage of tau protein in mice harboring the SREBP-2 transgene. (**A**) Representative immunoblot of total tau showing cleaved tau presence in brain extracts from SREBP-2 and APP/PS1/SREBP-2 mice at the indicated ages. (**B**) Western blot analysis of calpain activity by means of increase in the 145/150 kDa specific spectrin cleaved products. Quantification of the 145/150:240 kDa spectrin ratio exhibited a significant calpain activity increase in brain extracts from 7-month-old mutant mice compared with WT mice. (**C**) Representative protein immunoblot of cathepsin D (33 and 48 kDa, mature and immature forms, respectively) from brain extracts of 7-month-old WT and indicated mutant mice. Quantification of the 33:48 kDa ratio indicates an increased processing of cathepsin D in cerebral extracts from SREBP-2 and APP/PS1/SREBP-2 mice. (**D**) Cathepsin D activity analyzed in brain extracts from WT and transgenic mice (AUs). $^{*}P < 0.05$ versus WT values ($n = 3$). Values are expressed as mean $\pm$ S.D.

As seen, calpain-cleaved spectrin immunoreactivity and the subsequent quantification of the 150/145–240 kDa spectrin ratio in brain lysates indicated increased calpain activation in all three groups of mutant mice (SREBP-2, APP/PS1 and APP/PS1/SREBP-2 mice) compared with WT mice (Fig. 7B). The levels and activity of the lysosomal aspartic peptidase cathepsin D were also analyzed (Fig. 7C). We observed an upregulated expression of the immature form of cathepsin D (48 kDa) in all three mutant mice however, the ratio between mature and immature forms (33/48 kDa ratio) revealed an enhanced processing only in brain from mice that overexpress SREBP-2 (Fig. 7C). Although maturation seemed to be promoted by high levels of cholesterol, the increased levels of mature cathepsin D did not ultimately translate into a significant increase of enzyme activity (Fig. 7D). Therefore, these data suggest that neither calpain nor cathepsin D is responsible for tau cleavage in mice that carry the SREBP-2 transgene. The enhanced maturation of cathepsin D in these mice is more likely a compensatory response to an impaired endolysosome system, as previously reported using rabbits fed with a cholesterol-enriched diet (45), and hence, further work would be needed to elucidate the exact mechanism.

### Recovery of mGSH by *in vivo* GSH ethyl ester treatment reduces tau pathology and prevents amyloid plaques formation in APP/PS1/SREBP-2 mice

Since reactive oxygen species (ROS) can regulate major cellular signaling pathways, and particularly the activity of some members of the MAPK cascade (46), we next probed the potential mechanistic link between increased oxidative stress

and the progression of tau pathology in APP/PS1/SREBP-2 mice by treating mice with the cell-permeable derivative GSH ethyl ester (GSHee) (i.p. 1.25 mmol/kg/day, every 12 h for 2 weeks) (Fig. 8). As seen, GSHee administration significantly recovered the mitochondrial pool of GSH (Fig. 8A) and reduced the protein carbonyl content in brain from 7--month-old APP/PS1/SREBP-2 mice (Fig. 8B). Associated with this lower oxidative damage, we found decreased levels of phosphorylation in all the three MAPK analyzed, such as SAPK/JNK, ERK 1/2 and p38 MAPK (Fig. 8C), whereas the degree of phosphorylation in GSK-3β and CDK5 was unaltered in APP/PS1/SREBP-2 mice after GSHee administration (Fig. 8D). Interestingly, the inactivation of MAPK in the triple transgenic mice after mGSH recovery was sufficient to reduce the levels of tau phosphorylation at Ser-396 (Fig. 8E) and tau aggregation, with decreased levels of sarkosyl-insoluble tau in APP/PS1/SREBP-2 mice treated with GSHee (Fig. 8E). Previous experimental data indicated that oxidative stress can also modulate amyloid plaque pathology (47–49). We first examined whether mGSH recovery had any impact on the amyloidogenic processing of APP (Fig. 8G). As seen, levels of APP β-C-terminal fragments (β-CFTs) remained unchanged in the triple transgenic mice after GSHee treatment. However, GSHee significantly lowered the amyloid deposition detected by Aβ (1-42) antibody staining in hippocampal slices from APP/PS1/SREBP-2 mice (Fig. 8H and J). A similar degree of amyloid burden reduction was observed with thioflavin S staining (Fig. 8I and J). Since thioflavin S can also recognize and bind β-sheet pleated tau fibrils, we analyzed the images at higher magnification (Supplementary Material, Fig. S6) and found that GSHee treatment reduced the presence of thioflavin-positive structures in the pyramidal cell layers of the hippocampus was significantly reduced after GSHee administration. Moreover, the analyses of synaptophysin immunoreactivity showed that GSHee administration was able to significantly prevent the synaptic degeneration observed in triple transgenic mice at 7 months of age (Fig. 8K). Overall, these data show that alterations in brain cholesterol levels directly impact on AD progression. Mitochondrial oxidative stress can control tau phosphorylation via MAPK activation and cholesterol-induced mGSH depletion arises as a key pathogenic factor in AD, at least in part, by promoting tau pathology and Aβ deposition.

## DISCUSSION

Although cumulating evidence indicates that cholesterol can regulate Aβ accumulation and neurotoxicity, our current understanding of the underlying mechanisms and impact on AD is still incomplete. Here, we have generated a new AD mouse model that provides a unique tool to examine the age-dependent contribution of increased cholesterol in the onset of AD-like pathological alterations. A key feature of the triple transgenic model is the combined exhibition of amyloidogenic APP processing leading to Aβ generation and tau pathology due to SREBP-2 expression. Moreover, SREBP-2 expression in APP/PS1 mice accelerates and worsens brain oxidative damage and neuroinflammation, with an enhanced age-dependent synaptic degeneration already detectable in 4-month-old mice and neuronal death observed at 10 months of age. This outcome translated in spatial and object-recognition memory deficits, indicating a functional deterioration of perirhinal cortex and hippocampus.

Since triple transgenic mice exhibited stimulated Aβ synthesis and deposition in hippocampus at 4 months of age, much earlier than APP/PS1 mice, it could be speculated that the accelerated pathology observed in these mice is a merely consequence of increased amyloidogenesis. However, the fact that only APP/PS1 mice that carry the SREBP-2 transgene displayed frank neurodegeneration and recognition memory impairment at the age of 10 months, despite similar Aβ accumulation between APP/PS1 mice and triple transgenic mice, suggests the existence of other contributory mechanisms.

Associated with changes in brain cholesterol levels APP/PS1/SREBP-2 mice showed depleted mGSH. Therefore, given the key role of mGSH in controlling the oxidative stress generated in mitochondria (50), and based in our previous works that described an increased sensitivity to Aβ toxicity by mGSH-depleted cells (5,17), we hypothesized that a critical culprit in the neuronal death observed in the triple transgenic mice resulted from this compromised mitochondrial antioxidant defense. Additionally, recent studies suggest that mitochondrial dysfunction can promote tau hyperphosphorylation and neurodegeneration (22,51). Furthermore, tangle pathology rather than Aβ burden has been shown to correlate better with AD severity (52,53). While APP/PS1 mice do not exhibit the full spectrum of neurodegeneration, cognitive decline associated with synaptic dysfunction and neuronal loss has been reported in animal models expressing pro-aggregant tau (54,55). Furthermore, in these mice tau-mediated toxicity is reversed when aggregation is avoided (54,55). Remarkably, unlike other AD mouse models that require the expression of mutant human tau (56), we provide evidence that APP/PS1/SREBP-2 mice developed full tau pathology.

A link between cholesterol and tau pathology reflected by NFT has been previously observed in brains from individuals affected by the lipid storage disorder NPC (57,58). Further studies in mouse models of NPC show that impaired cellular cholesterol trafficking is associated with enhanced generation of Aβ and the hyperphosphorylation of tau, mirroring AD pathology (28,39,59). Conversely, treatment with cyclodextin ameliorates Aβ and tau alterations, resulting in delayed neurodegeneration and increased lifespan of NPC mice (31,60,61). In the same line, we observed an early phosphorylation of endogenous tau in epitopes linked to tangle formation associated with the presence of Gallyas/thioflavin S-positive neurons in the hippocampus of APP/PS1/SREBP-2 mice, indicative of AD-type NFTs. Evidence to support this outcome included the presence of sarkosyl-insoluble tau accumulation reflecting the onset of tau aggregates. Moreover, using a phospho-specific tau antibody we showed that these structures accumulate in the somatodendritic compartment of hippocampal neurons, in agreement with previous reports describing a missorting of tau from the normal axonal localization to somatodendritic sites in AD brain (62,63). Whether tau inclusions are toxic, interfere in essential cell processes or trigger neurite degeneration by decreasing microtubule stabilization is still under debate. Moreover, a growing body of evidence also point to pre-tangle tau species (soluble monomers or oligomers) as the main

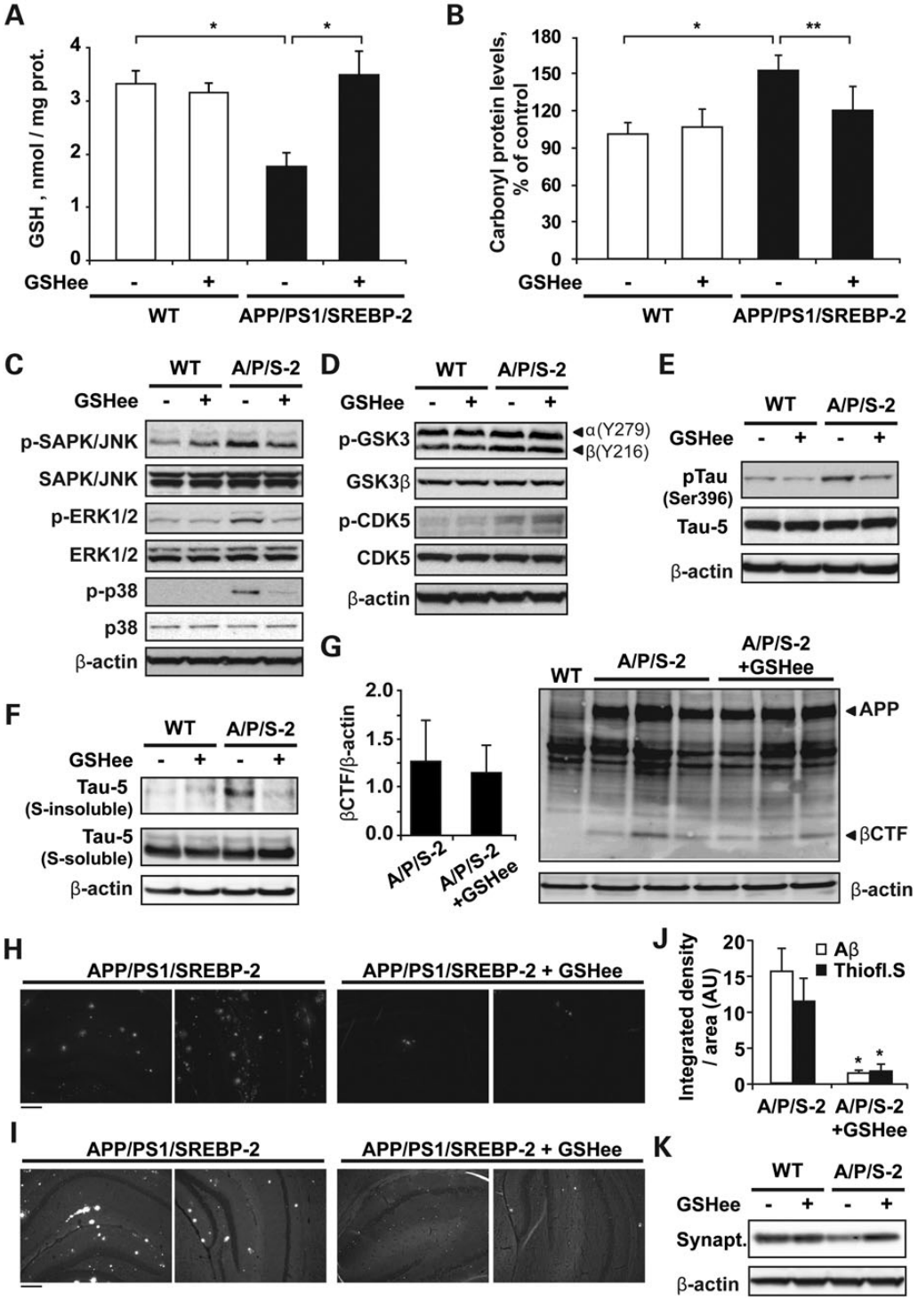


**Figure 8.** *In vivo* GSH ethyl ester treatment recovers mGSH and prevents tau pathology and Aβ deposition in APP/PS1/SREBP-2 mice. 7-month-old WT and APP/PS1/SREBP-2 mice were treated with GSH ethyl ester (GSHee; i.p. 1.25 mmol/kg/day) for 2 weeks. (**A** and **B**) Mitochondrial GSH levels and the protein carbonyl content after GSHee therapy. $^{*}P < 0.01$, $^{**}P < 0.05$ ($n = 6$). Values are expressed as mean ± SD. (**C**) Representative immunoblots (non-phosphorylated and active phosphorylated forms) of JNK/SAPK, ERK 1/2, and p38 MAP kinases showing reduced activation in brain extracts of APP/PS1/SREBP-2 mice after GSHee treatment. (**D**) Western blot analysis of GSK-3β activation with antibodies against Y279 and Y216 (activating sites) and CDK5 phosphorylation showing an enhanced activity of both kinases in APP/PS1/SREBP-2 mice independently of GSHee treatment. (**E**) Representative immunoblots showing reduced tau phosphorylation at Ser 396 in brain extracts of APP/PS1/SREBP-2 mice after GSHee treatment. Total tau levels were detected by the phosphorylation-independent antibody Tau-5. (**F**) Protein immunoblots of total tau (Tau-5) in crude (s-soluble) and sarcosyl-insoluble (s-insoluble) fractions showing decreased presence of insoluble tau in APP/PS1/SREBP-2 mice after GSHee treatment. (**G**) Western blot analysis of β-CTFs using Aβ antibody (clone 6E10). The levels of β-CFTs were normalized to β-actin (left graph). (**H** and **I**) Representative immunofluorescent images of amyloid plaques stained with an Aβ antibody (clone 6E10) (H) and thioflavin S (I). (**J**) Quantification of Aβ immunoreactivity and thioflavin staining by integrated density analysis showing decreased amyloid burden in hippocampus from APP/PS1/SREBP-2 mice after GSHee treatment. (AUs). $^{*}P < 0.001$ ($n = 4$). Values are expressed as mean ± SD. (**K**) Representative immunoblot of synaptophysin (synapt.) protein levels.

responsible for toxicity in tauopathies (64). Therefore, further research is needed to understand the exact mechanisms by which tau contributes to disease.

SREBP-2 transgenic mice did not develop NFTs, indicating that the rise of cholesterol levels and its trafficking to mitochondria to elicit mGSH depletion *per se* are not sufficient to promote tau hyperphosphorylation and aggregation. Many studies have previously reported the potentiation of tau pathology by Aβ, positioning tau abnormalities downstream of Aβ in AD (20,65,66). Accordingly, our results show that generation of Aβ and mitochondrial cholesterol-induced mGSH depletion are required for the oxidative stress-mediated activation of tau kinases, particularly, MAP kinases, which in turn participate in the cascade of events leading to tau aggregation. In line with this scenario, mGSH recovery by GSH ethyl ester prevented MAP kinases activation and tau phosphorylation in triple transgenic mice. Although CDK5 and GSK3β were also activated in APP/PS1/SREBP-2 mice their activity, unlike that of MAP kinases, remained unaltered after blocking Aβ-induced oxidative stress by GSH ethyl ester treatment. Recent evidence indicates that both CDK5 and GSK3β are activated on cellular membranes, and thus deregulation of sterol may somehow modulate their activity by poorly understood mechanisms (67,68). Moreover, we did not find any changes in the phosphorylation state nor in the expression of the catalytic subunit of the PP2A, indicating that although cholesterol may stimulate tau kinases activation, phosphatase activity is not influenced by cholesterol load, as previously described (33), hence suggesting a minor role of PP2A in cholesterol-induced tau pathology.

Quite intriguingly, the levels of brain cholesterol in 10 month-old APP/PS1 mice were similar to those observed in the triple transgenic mice. Yet, only the latter exhibited tau pathology and neurodegeneration. Perhaps a key clue to this apparent riddle may involve the different mechanisms of cholesterol accumulation between APP/PS1 mice driven by Aβ and the triple transgenic mice due to SREBP-2 expression. While Aβ-mediated cholesterol regulation involves low density lipoprotein receptor-related protein 1 (14), SREBP-2 is a key transcription factor regulating the synthesis of cholesterol in the mevalonate pathway (69). In addition to synthesizing cholesterol, the mevalonate pathway is also essential in the generation of isoprenoids and hence in protein prenylation, a key post-translational mechanism of proteins. While targeting protein prenylation has been shown to be of potential relevance in cancer cell biology (70), emerging evidence reports alteration in the regulation of isoprenoids farnesyl- and geranylgeranylpyrophosphate (GGPP) in patients with AD (71). Moreover, recent data in a cellular model of tauopathy show that statin-induced inhibition of GGPP decreases phosphorylated tau levels by affecting GSK3β activity (72). Hence, it is conceivable that triple transgenic mice exhibit increased protein prenylation with respect to APP/PS1 that may contribute to tau pathology. High circulating cholesterol levels in APP/PS1/SREBP-2 mice might also play an additive role as treatment with different types of statins has been described to reduce NFT severity regardless of the capability to cross the blood–brain barrier (73).

APP/PS1 mice exhibit spatial memory deficits in the absence of neuronal loss and in agreement with previous reports showing a correlation between the degree of cognitive impairment and synaptic dysfunction (74). Moreover, when we analyzed the contribution of cholesterol in cognition we observed that SREBP-2 overexpression in APP/PS1 mice did not worsen the loss of spatial memory retention but impaired novel object recognition ability. Interestingly, this short-term recognition memory mainly relays on the perirhinal cortex (37,38). Furthermore, histological studies and magnetic resonance image analysis demonstrate that pathological changes involve the entorhinal and perirhinal cortex early in the course of the disease (75,76), with NFTs described to first develop in these brain areas before spreading to the hippocampus (75,77).

Recently, different reports using specific mitochondria-targeted antioxidants suggest that protection of mitochondrial function is sufficient to prevent AD-like neuropathology (78,79). Our *in vivo* treatment with GSH ethyl ester further supports a central role of mitochondrial oxidative stress in the neurodegenerative process. We found that administration of GSH ethyl ester to APP/PS1/SREBP-2 mice for 2 weeks was sufficient to recover the pool of mGSH resulting in significant reduction in the carbonyl protein levels. Associated with this decreased oxidative damage, we observed an improvement in tau pathology and increased synaptophysin levels, indicative of synaptic recovery. Moreover, our findings are consistent with previous studies in Tg19959 mice, showing that overexpression of the mitochondrial antioxidant enzyme manganese superoxide dismutase reduces amyloid plaque burden without alteration in amyloidogenic processing (49). In addition, although tau pathology was not addressed in these mice, synaptophysin levels and spatial memory deficits were restored to WT levels (49). Based on recent findings indicating that mGSH determines the therapeutic potential of superoxide anion scavenging in steatohepatitis (80), it remains to be established whether the beneficial effects of MnSOD overexpression in Tg19959 mice was dependent on mGSH levels. Overall, our results provide novel insights into the relationship between cholesterol and the disease progression, underlining the key contributory role of an impaired cholesterol homeostasis in tau pathology and consistent with recent studies, providing evidence for the use of mitochondria-targeted therapeutics directed to protect the mitochondrial antioxidant defense.

## MATERIALS AND METHODS

### APP/PS1 and SREBP-2 mice

Breeding pairs of B6C3-Tg(APPswe,PSEN1dE9)85Dbo/J and B6;SJL-Tg(rPEPCKSREBF2)788Reh/J were purchased from The Jackson Laboratory. APP/PS1/SREBP-2 mice were generated from crossbreeding SREBP-2 and APP/PS1 mice, which were first back-crossed more than five generations into the B6SJL background. At the time of weaning (21 days), mice were genetically identified by PCR using DNA from ear tips and following the genotyping protocols provided by the supplier. Male mice at the indicated ages of different genotypes used in a given experiment were obtained from the same breeding pairs. All procedures involving animals and their care were approved by the ethics committee of the University of Barcelona and were conducted in accordance with institutional guidelines in compliance with national and international laws and policies.

### Mitochondrial isolation

Cerebral cortices were isolated and homogenized in 210 mM mannitol, 60 mM sucrose, 10 mM KCl, 10 mM sodium succinate, 1 mM ADP, 0.25 mM DTT, 0.1 mM EGTA, 10 mM HEPES, pH 7.4. Homogenates were centrifuged at 700*g* for 10 min, with the recovered supernatant being centrifuged at 10 000*g* for 15 min. The resulting pellet was suspended in 2 ml, loaded onto 8 ml of 30% (v/v) percoll gradient and centrifuged at 95 000*g* for 30 min. The mitochondrial pellet was then rinsed twice by centrifuging 15 min at 10 000*g*.

### GSH and cholesterol measurements

GSH levels in homogenates and mitochondria were analyzed by the recycling method (81). For cholesterol determination, samples were extracted with alcoholic KOH, distilled water and hexane (1:1:2, v/v/v). Appropriate aliquots of the hexane layer were evaporated and used for cholesterol measurement (82). HPLC analysis was made using a Waters μBondapak C18 10 μm reversed-phase column (30 cm × 4 mm inner diameter), with the mobile phase being 2-propanol/acetonitrile/distilled water (6:3:1, v/v/v) at a flow rate of 1 ml/min. The amount of cholesterol was calculated from standard curves, and the identity of the peaks was confirmed by spiking the sample with known standards.

### β-Secretase activity, cathepsin D activity and Aβ levels

β-Secretase and cathepsin D activities were analyzed spectrofluorometrically using commercial assay kits from Abcam. Levels of endogenous or human recombinant Aβ1-42 peptides in brain extracts were determined in duplicate using the colorimetric mouse and human Aβ1-42 ELISA kits (Biosource International) following the manufacturer's instructions.

### Carbonyl protein levels

Protein carbonylation was estimated using the Oxyblot™ protein oxidation detection kit (Chemicon) according to the manufacturer's instructions. Briefly, the carbonyl groups in the protein side chains were derivatized by reaction with 2,4-dinitrophenylhydrazine (DNPH), and the DNP derivatives were analyzed by western blotting. In parallel, samples were examined spectrophotometrically using the OxiSelect™ protein carbonyl spectrophotometric assay kit (Cell Biolabs).

### Western blot analysis

Samples (30–80 μg of protein/lane) were resolved by SDS-PAGE and transferred to nitrocellulose membranes. Blots were probed with antibodies listed in Table 2. After overnight incubation at 4°C, bound antibodies were visualized using horseradish peroxidase-coupled secondary antibodies and ECL developing kits (Amersham Biosciences). Densitometry of the bands was measured with QuantityOne software and the values were normalized to β-actin or glyceraldehyde-3-phosphate dehydrogenase (GAPDH).

Sarcosyl insoluble tau was isolated based on the modified method of Greenberg and Davies (83). Brain tissue was homogenized in tris-buffered saline (TBS), a small sample was removed for the analysis of total tau and the remainder was centrifuged at 100 000*g* for 60 min at 4°C. The pellet was homogenized in 0.8 M NaCl and 10% sucrose in TBS. After centrifugation at 150 000*g* for 15 min, the supernatant was brought to 1% sarkosyl and incubated at 37°C for 1 h. The mixture was then centrifuged at 150 000*g* for 30 min and the precipitate was collected as the sarkosyl-insoluble fraction.

### Immunohistochemistry

Cryopreserved (10 μm) or paraffin (5 μm) sections from −1.2 mm through −2.4 mm from Bregma were processed according to the avidin–biotin–peroxidase staining method (Vectastain ABC kit; Vector Lab). Tissues processed for Aβ staining were pretreated with 99% formic acid for 7 min. After antigen retrieval treatment, the endogenous peroxidase was blocked by exposure to 3% $H_2O_2$ in methanol for 30 min. The sections were treated with the Avidin/Biotin blocking kit from Vector Lab according to the manufacturer's instructions and incubated overnight at 4°C with antibodies listed in Table 2. After washing with phosphate buffered saline (PBS), sections were then incubated for 1 h with appropriated biotinylated secondary antibodies at a dilution of 1:400, followed by ABC staining for 1 h. The immunoreaction was visualized with diaminobenzidine (DAB enhanced liquid substrate system, Sigma). Sections were counterstained with hematoxylin (Dako). The presence of NFTs was detected by Gallyas silver staining. To analyze the presence of β-sheet-rich structures, sections were stained in 1% Thioflavine S for 5 min, and differentiated with 70% ethanol for 5 min. To detect DNA fragmentation, terminal deoxynucleotidyl transferase-mediated uridine 5′-triphosphate-biotin nick end-labeling (TUNEL assay) was performed according to the manufacturer's recommendations (*In Situ* Cell Death Detection Kit, TUNEL POD, Roche Applied Science). Neuronal degeneration was also assessed by staining sections with Fluoro-Jade B (0.0004%, Chemicon) (84).

### Immunofluorescence and laser confocal imaging

Dewaxed hippocampal sections were first boiled in citrate buffer (10 mM sodium citrate pH 6.0) and incubated with 0.1 M glycine/PBS for 20 min to reduce autofluorescence. The sections were incubated overnight at 4°C with antibodies listed in Table 2. After washing in PBS, antibody staining was visualized using Alexa 488- and Cy3-coupled secondary antibodies (1:400; Invitrogen and Jackson ImmunoResearch Inc.). In some cases, nuclei were stained with Hoechst 33258 (2 μg/ml) before mounting the samples in Fluoromount-G (Southern Biotech). Confocal images were collected using a Leica TCS SPE laser scanning confocal microscope equipped with UV excitation, an argon laser, a 633/1.32 OIL PH3 CS objective and a confocal pinhole set at 1 Airy unit. All the confocal images shown were single optical sections. For GFAP and F4/80 integrated density analysis, nonsaturated images from equivalent regions were analyzed with ImageJ software to quantify integrated density staining per relevant area within each image for each replicate. Threshold adjustments were set to ensure quantification of only positive immunostaining.

**Table 2.** Details of the primary antibodies used in this study

| Antibody | Source and type | Company | WB dilution | IHC/IF dilution |
|---|---|---|---|---|
| 8-Hydroxyguanosine | Goat polyclonal | Calbiochem | | 1:200 |
| A$\beta$ human (6E10) | Mouse monoclonal | Sigma-Aldrich | 1:1000 | 1:300 |
| Cathepsin D | Goat polyclonal | Santa Cruz Biotech | 1:500 | |
| CDK5 | Rabbit polyclonal | Santa Cruz Biotech | 1:500 | |
| ERK1/2 | Rabbit polyclonal | Cell Signaling | 1:1000 | |
| F4/80 | Rat monoclonal | Santa Cruz Biotech | | 1:200 |
| GAPDH (6C5) | Mouse monoclonal | Santa Cruz Biotech | 1:5000 | |
| GFAP | Rabbit polyclonal | Dako | | 1:500 |
| GSK3$\beta$ | Rabbit monoclonal | Cell Signaling | 1:1000 | |
| MAP2 | Rabbit polyclonal | Chemicon (Millipore) | | 1:500 |
| MBP | Rat monoclonal | Chemicon (Millipore) | | 1:500 |
| p35 (C-19) | Rabbit polyclonal | Santa Cruz Biotech | 1:200 | |
| p38 MAPK | Rabbit polyclonal | Cell Signaling | 1:1000 | |
| PHF-Tau (AT8) | Mouse monoclonal | BioScience | 1:1000 | 1:200 |
| Phospho-CDK5 (Tyr15) | Rabbit polyclonal | Santa Cruz Biotech | 1:500 | |
| Phospho-ERK1/2 (Thr202/Tyr204) | Mouse monoclonal | Cell Signaling | 1:1000 | |
| Phospho-GSK3$\beta$ (Ser9) | Rabbit monoclonal | Cell Signaling | 1:1000 | |
| Phospho-GSK3 $\alpha$(Y279)/$\beta$(Y216) | Rabbit polyclonal | Invitrogen | 1:1000 | |
| Phospho-p38 MAPK (Thr180/Tyr182) | Mouse monoclonal | Cell Signaling | 1:1000 | |
| Phospho-SAPK/JNK (Thr183/Tyr185) | Rabbit monoclonal | Cell Signaling | 1:1000 | |
| Phospho-Tau (Ser396) | Rabbit polyclonal | Santa Cruz Biotech | 1:200 | |
| PP2A (C subunit) | Mouse monoclonal | Upstate (Millipore) | 1:1000 | |
| PP2A C$\alpha/\beta$ | Mouse monoclonal | Santa Cruz Biotech | 1:500 | |
| SAPK/JNK | Rabbit polyclonal | Cell Signaling | 1:1000 | |
| Spectrin (AA6) | Mouse monoclonal | Chemicon (Millipore) | 1:1000 | |
| Synaptophysine | Rabbit polyclonal | Abcam | 1:1000 | |
| Tau (TAU-5) | Mouse monoclonal | Invitrogen | 1:1000 | |
| $\beta$-actin | Mouse monoclonal | Sigma-Aldrich | 1:10 000 | |

### Real-time RT-PCR

Total RNA was isolated from brain with the TRIzol reagent (Invitrogen). Real-time PCR amplification for IL-1β was performed using the iScript™ One-Step RT-PCR kit with SYBR® Green (Bio-Rad) following the manufacturer's protocol. Briefly, 20 ng of total RNA, 600 μmol/l of primers and 12.5 μl of 2× reaction mix were incubated in 25 μl at 50°C for 10 and 95°C for 5 min, followed by 45 cycles of 95°C for 10 s, 56°C for 30 s, and 72°C for 30 s. Each reaction was run in duplicate, and the threshold (CT) values for each mRNA were subtracted from that of 18S mRNA, averaged and converted from log-linear to linear term. The primers used were: IL-1β forward 5′-GAGCTGAAAGCTCTCCACCTC-3′; IL-1β reverse 5′-CTTTCCTTTGAGGCCCAAGGC-3′; 18s forward 5′-GTAACCCGTTGAACCCCATT-3′; 18s reverse 5′-CCATCCAATCGGTAGTAGCG -3′.

### Morris water maze

Hippocampus-dependent spatial memory was examined using the MWM (85). Briefly, the water-maze pool (diameter, 100 cm) contained opaque water (23 ± 1°C) with a platform (diameter, 10 cm) submerged 1 cm. To evaluate the visual perception and motivation, mice were trained to locate first a cued platform (Sessions 1 and 2). To test reference memory, mice were trained using a hidden platform with four visual cues surrounding the pool of water and limiting the four quadrants (Sessions 3–7). The platform was located in the center of one of the quadrants of the pool (target quadrant). Animals were allowed 60 s to locate the platform and 30 s to rest on it. Mice that failed to find the platform were placed on it and allowed to rest there for 30 s. The acquisition task consisted in eight trials per day with 15 min inter-trial intervals. To assess spatial memory retention, a single 60 s probe trial without platform was administered 1 h after the last hidden-platform session. Performance was recorded with an automated tracking system (SmartJunior) during all training and probe trials. The relative time spent in each of the four quadrants and the number of crossings of the former platform location were recorded and analyzed during the probe trials.

### Novel object recognition

The novel object recognition task, which uses cortical and hippocampal inputs, was administered as described (86). During three consecutive days, mice were habituated to an empty open field (diameter, 40 cm) for 10 min. The fourth day, mice were allowed to explore two identical objects located equidistant from the walls and the center of the open field during 10 min. One hour later, the trial was repeated with one of the objects being replaced with a novel object of similar size. The time spent exploring the identical and novel objects was quantified. Between each trial, the open field was cleaned with 70% ethanol to eliminate olfactory cues. An increased percentage of time spent exploring the novel object (duration spent with the novel object)/(duration spent with the novel object + duration spent with familiar object) × 100) is considered an index of enhanced cognitive performance in this task.

### Statistics

Results are expressed as means ± SD of the number of experiments. Statistical significance was examined using the unpaired

two-tailed Student's *t*-test or one-way ANOVA with Dunnett's or Bonferroni's *post hoc* multiple comparisons test when required. A *P*-value of $<0.05$ was considered statistically significant.

## SUPPLEMENTARY MATERIAL

Supplementary Material is available at *HMG* online.

## ACKNOWLEDGEMENTS

We thank Drs C. García-Ruiz, M. Marí and A. Morales for valuable suggestions and input. This work was developed (in part) at the Centre Esther Koplowitz.

*Conflict of Interest statement*. None declared.

## FUNDING

This work was supported by Plan Nacional de I + D + I (SAF2010-03923 to A.C. and SAF2009-11417 and SAF2012-34831 to J.C.F-C); by Centro de Investigacion Biomedica en Red de Enfermedades Hepaticas y Digestivas (CIBEREHD); by Instituto de Salud Carlos III; by Research Center for Liver and Pancreatic Diseases, NIAAA/NIH (P50-AA-11999 to J.C. F-C) and by Marato TV3. E.B.C. has a FPI fellowship from Ministerio de Economía y Competitividad.

## REFERENCES

1. Cutler, R.G., Kelly, J., Storie, K., Pedersen, W.A., Tammara, A., Hatanpaa, K., Troncoso, J.C. and Mattson, M.P. (2004) Involvement of oxidative stress-induced abnormalities in ceramide and cholesterol metabolism in brain aging and Alzheimer's disease. *Proc. Natl Acad. Sci. USA*, **101**, 2070–2075.
2. Bandaru, V.V., Troncoso, J., Wheeler, D., Pletnikova, O., Wang, J., Conant, K. and Haughey, N.J. (2009) ApoE4 disrupts sterol and sphingolipid metabolism in Alzheimer's but not normal brain. *Neurobiol. Aging*, **30**, 591–599.
3. Xiong, H., Callaghan, D., Jones, A., Walker, D.G., Lue, L.F., Beach, T.G., Sue, L.I., Woulfe, J., Xu, H., Stanimirovic, D.B. *et al.* (2008) Cholesterol retention in Alzheimer's brain is responsible for high beta- and gamma-secretase activities and Abeta production. *Neurobiol. Dis.*, **29**, 422–437.
4. Panchal, M., Loeper, J., Cossec, J.C., Perruchini, C., Lazar, A., Pompon, D. and Duyckaerts, C. (2010) Enrichment of cholesterol in microdissected Alzheimer's disease senile plaques as assessed by mass spectrometry. *J. Lipid Res.*, **51**, 598–605.
5. Fernandez, A., Llacuna, L., Fernandez-Checa, J.C. and Colell, A. (2009) Mitochondrial cholesterol loading exacerbates amyloid beta peptide-induced inflammation and neurotoxicity. *J. Neurosci.*, **29**, 6394–6405.
6. Pfrieger, F.W. (2003) Cholesterol homeostasis and function in neurons of the central nervous system. *Cell Mol. Life Sci.*, **60**, 1158–1171.
7. Shepardson, N.E., Shankar, G.M. and Selkoe, D.J. (2011) Cholesterol level and statin use in Alzheimer disease: I. Review of epidemiological and preclinical studies. *Arch. Neurol.*, **68**, 1239–1244.
8. Ehehalt, R., Keller, P., Haass, C., Thiele, C. and Simons, K. (2003) Amyloidogenic processing of the Alzheimer beta-amyloid precursor protein depends on lipid rafts. *J. Cell Biol.*, **160**, 113–123.
9. Kalvodova, L., Kahya, N., Schwille, P., Ehehalt, R., Verkade, P., Drechsel, D. and Simons, K. (2005) Lipids as modulators of proteolytic activity of BACE: involvement of cholesterol, glycosphingolipids, and anionic phospholipids *in vitro*. *J. Biol. Chem.*, **280**, 36815–36823.
10. Osenkowski, P., Ye, W., Wang, R., Wolfe, M.S. and Selkoe, D.J. (2008) Direct and potent regulation of gamma-secretase by its lipid microenvironment. *J. Biol. Chem.*, **283**, 22529–22540.
11. Yip, C.M., Elton, E.A., Darabie, A.A., Morrison, M.R. and McLaurin, J. (2001) Cholesterol, a modulator of membrane-associated Abeta-fibrillogenesis and neurotoxicity. *J. Mol. Biol.*, **311**, 723–734.
12. Lee, C.Y., Tse, W., Smith, J.D. and Landreth, G.E. (2012) Apolipoprotein E promotes beta-amyloid trafficking and degradation by modulating microglial cholesterol levels. *J. Biol. Chem.*, **287**, 2032–2044.
13. Grimm, M.O., Grimm, H.S., Patzold, A.J., Zinser, E.G., Halonen, R., Duering, M., Tschape, J.A., De Strooper, B., Muller, U., Shen, J. *et al.* (2005) Regulation of cholesterol and sphingomyelin metabolism by amyloid-beta and presenilin. *Nat. Cell Biol.*, **7**, 1118–1123.
14. Liu, Q., Zerbinatti, C.V., Zhang, J., Hoe, H.S., Wang, B., Cole, S.L., Herz, J., Muglia, L. and Bu, G. (2007) Amyloid precursor protein regulates brain apolipoprotein E and cholesterol metabolism through lipoprotein receptor LRP1. *Neuron*, **56**, 66–78.
15. Bryleva, E.Y., Rogers, M.A., Chang, C.C., Buen, F., Harris, B.T., Rousselet, E., Seidah, N.G., Oddo, S., LaFerla, F.M., Spencer, T.A. *et al.* (2010) ACAT1 gene ablation increases 24(S)-hydroxycholesterol content in the brain and ameliorates amyloid pathology in mice with AD. *Proc. Natl Acad. Sci. USA*, **107**, 3081–3086.
16. Yao, J., Ho, D., Calingasan, N.Y., Pipalia, N.H., Lin, M.T. and Beal, M.F. (2012) Neuroprotection by cyclodextrin in cell and mouse models of Alzheimer disease. *J. Exp. Med.*, **209**, 2501–2513.
17. Colell, A., Fernandez, A. and Fernandez-Checa, J.C. (2009) Mitochondria, cholesterol and amyloid beta peptide: a dangerous trio in Alzheimer disease. *J. Bioenerg. Biomembr.*, **41**, 417–423.
18. Ashe, K.H. and Zahs, K.R. (2010) Probing the biology of Alzheimer's disease in mice. *Neuron*, **66**, 631–645.
19. Chabrier, M.A., Blurton-Jones, M., Agazaryan, A.A., Nerhus, J.L., Martinez-Coria, H. and LaFerla, F.M. (2012) Soluble abeta promotes wild-type tau pathology *in vivo*. *J. Neurosci.*, **32**, 17345–17350.
20. Jin, M., Shepardson, N., Yang, T., Chen, G., Walsh, D. and Selkoe, D.J. (2011) Soluble amyloid beta-protein dimers isolated from Alzheimer cortex directly induce Tau hyperphosphorylation and neuritic degeneration. *Proc. Natl Acad. Sci. USA*, **108**, 5819–5824.
21. Tokutake, T., Kasuga, K., Yajima, R., Sekine, Y., Tezuka, T., Nishizawa, M. and Ikeuchi, T. (2012) Hyperphosphorylation of Tau induced by naturally secreted amyloid-beta at nanomolar concentrations is modulated by insulin-dependent Akt-GSK3beta signaling pathway. *J. Biol. Chem.*, **287**, 35222–35233.
22. Melov, S., Adlard, P.A., Morten, K., Johnson, F., Golden, T.R., Hinerfeld, D., Schilling, B., Mavros, C., Masters, C.L., Volitakis, I. *et al.* (2007) Mitochondrial oxidative stress causes hyperphosphorylation of tau. *PLoS One*, **2**, e536.
23. Iijima-Ando, K., Sekiya, M., Maruko-Otake, A., Ohtake, Y., Suzuki, E., Lu, B. and Iijima, K.M. (2012) Loss of axonal mitochondria promotes tau-mediated neurodegeneration and Alzheimer's disease-related tau phosphorylation via PAR-1. *PLoS Genet*, **8**, e1002918.
24. DuBoff, B., Gotz, J. and Feany, M.B. (2012) Tau promotes neurodegeneration via DRP1 mislocalization *in vivo*. *Neuron*, **75**, 618–632.
25. Distl, R., Meske, V. and Ohm, T.G. (2001) Tangle-bearing neurons contain more free cholesterol than adjacent tangle-free neurons. *Acta Neuropathol.*, **101**, 547–554.
26. Love, S., Bridges, L.R. and Case, C.P. (1995) Neurofibrillary tangles in Niemann-Pick disease type C. *Brain*, **118** (Pt 1), 119–129.
27. Yu, W., Gong, J.S., Ko, M., Garver, W.S., Yanagisawa, K. and Michikawa, M. (2005) Altered cholesterol metabolism in Niemann-Pick type C1 mouse brains affects mitochondrial function. *J. Biol. Chem.*, **280**, 11731–11739.
28. Sawamura, N., Gong, J.S., Garver, W.S., Heidenreich, R.A., Ninomiya, H., Ohno, K., Yanagisawa, K. and Michikawa, M. (2001) Site-specific phosphorylation of tau accompanied by activation of mitogen-activated protein kinase (MAPK) in brains of Niemann-Pick type C mice. *J. Biol. Chem.*, **276**, 10314–10319.
29. Burns, M., Gaynor, K., Olm, V., Mercken, M., LaFrancois, J., Wang, L., Mathews, P.M., Noble, W., Matsuoka, Y. and Duff, K. (2003) Presenilin redistribution associated with aberrant cholesterol transport enhances beta-amyloid production *in vivo*. *J. Neurosci.*, **23**, 5645–5649.
30. Kodam, A., Maulik, M., Peake, K., Amritraj, A., Vetrivel, K.S., Thinakaran, G., Vance, J.E. and Kar, S. (2010) Altered levels and distribution of amyloid precursor protein and its processing enzymes in Niemann-Pick type C1-deficient mouse brains. *Glia*, **58**, 1267–1281.

31. Maulik, M., Ghoshal, B., Kim, J., Wang, Y., Yang, J., Westaway, D. and Kar, S. (2012) Mutant human APP exacerbates pathology in a mouse model of NPC and its reversal by a beta-cyclodextrin. *Hum. Mol. Genet.*, **21**, 4857–4875.
32. Glockner, F., Meske, V., Lutjohann, D. and Ohm, T.G. (2011) Dietary cholesterol and its effect on tau protein: a study in apolipoprotein E-deficient and P301L human tau mice. *J. Neuropathol. Exp. Neurol.*, **70**, 292–301.
33. Rahman, A., Akterin, S., Flores-Morales, A., Crisby, M., Kivipelto, M., Schultzberg, M. and Cedazo-Minguez, A. (2005) High cholesterol diet induces tau hyperphosphorylation in apolipoprotein E deficient mice. *FEBS Lett.*, **579**, 6411–6416.
34. Games, D., Buttini, M., Kobayashi, D., Schenk, D. and Seubert, P. (2006) Mice as models: transgenic approaches and Alzheimer's disease. *J. Alzheimers Dis.*, **9**, 133–149.
35. Yang, D.S., Kumar, A., Stavrides, P., Peterson, J., Peterhoff, C.M., Pawlik, M., Levy, E., Cataldo, A.M. and Nixon, R.A. (2008) Neuronal apoptosis and autophagy cross talk in aging PS/APP mice, a model of Alzheimer's disease. *Am. J. Pathol.*, **173**, 665–681.
36. Sadowski, M., Pankiewicz, J., Scholtzova, H., Ji, Y., Quartermain, D., Jensen, C.H., Duff, K., Nixon, R.A., Gruen, R.J. and Wisniewski, T. (2004) Amyloid-beta deposition is associated with decreased hippocampal glucose metabolism and spatial memory impairment in APP/PS1 mice. *J. Neuropathol. Exp. Neurol.*, **63**, 418–428.
37. Brown, M.W. and Aggleton, J.P. (2001) Recognition memory: what are the roles of the perirhinal cortex and hippocampus? *Nat. Rev. Neurosci.*, **2**, 51–61.
38. Winters, B.D., Forwood, S.E., Cowell, R.A., Saksida, L.M. and Bussey, T.J. (2004) Double dissociation between the effects of peri-postrhinal cortex and hippocampal lesions on tests of object recognition and spatial memory: heterogeneity of function within the temporal lobe. *J. Neurosci.*, **24**, 5901–5908.
39. Mattsson, N., Olsson, M., Gustavsson, M.K., Kosicek, M., Malnar, M., Mansson, J.E., Blomqvist, M., Gobom, J., Andreasson, U., Brinkmalm, G. *et al.* (2012) Amyloid-beta metabolism in Niemann-Pick C disease models and patients. *Metab. Brain Dis.*, **27**, 573–585.
40. Nishimura, M., Tomimoto, H., Suenaga, T., Namba, Y., Ikeda, K., Akiguchi, I. and Kimura, J. (1995) Immunocytochemical characterization of glial fibrillary tangles in Alzheimer's disease brain. *Am. J. Pathol.*, **146**, 1052–1058.
41. Rudrabhatla, P. and Pant, H.C. (2011) Role of protein phosphatase 2A in Alzheimer's disease. *Curr. Alzheimer Res.*, **8**, 623–632.
42. Wang, Y.P., Biernat, J., Pickhardt, M., Mandelkow, E. and Mandelkow, E.M. (2007) Stepwise proteolysis liberates tau fragments that nucleate the Alzheimer-like aggregation of full-length tau in a neuronal cell model. *Proc. Natl Acad. Sci. USA*, **104**, 10252–10257.
43. Nicholson, A.M. and Ferreira, A. (2009) Increased membrane cholesterol might render mature hippocampal neurons more susceptible to beta-amyloid-induced calpain activation and tau toxicity. *J. Neurosci.*, **29**, 4640–4651.
44. Ma, T., Zhao, Y., Kwak, Y.D., Yang, Z., Thompson, R., Luo, Z., Xu, H. and Liao, F.F. (2009) Statin's excitoprotection is mediated by sAPP and the subsequent attenuation of calpain-induced truncation events, likely via rho-ROCK signaling. *J. Neurosci.*, **29**, 11226–11236.
45. Chen, X., Wagener, J.F., Morgan, D.H., Hui, L., Ghribi, O. and Geiger, J.D. (2010) Endolysosome mechanisms associated with Alzheimer's disease-like pathology in rabbits ingesting cholesterol-enriched diet. *J. Alzheimers Dis.*, **22**, 1289–1303.
46. Ray, P.D., Huang, B.W. and Tsuji, Y. (2012) Reactive oxygen species (ROS) homeostasis and redox regulation in cellular signaling. *Cell Signal*, **24**, 981–990.
47. Lim, G.P., Chu, T., Yang, F., Beech, W., Frautschy, S.A. and Cole, G.M. (2001) The curry spice curcumin reduces oxidative damage and amyloid pathology in an Alzheimer transgenic mouse. *J. Neurosci.*, **21**, 8370–8377.
48. Li, F., Calingasan, N.Y., Yu, F., Mauck, W.M., Toidze, M., Almeida, C.G., Takahashi, R.H., Carlson, G.A., Flint Beal, M., Lin, M.T. *et al.* (2004) Increased plaque burden in brains of APP mutant MnSOD heterozygous knockout mice. *J. Neurochem.*, **89**, 1308–1312.
49. Dumont, M., Wille, E., Stack, C., Calingasan, N.Y., Beal, M.F. and Lin, M.T. (2009) Reduction of oxidative stress, amyloid deposition, and memory deficit by manganese superoxide dismutase overexpression in a transgenic mouse model of Alzheimer's disease. *FASEB J.*, **23**, 2459–2466.
50. Mari, M., Morales, A., Colell, A., Garcia-Ruiz, C. and Fernandez-Checa, J.C. (2009) Mitochondrial glutathione, a key survival antioxidant. *Antioxid. Redox Signal.*, **11**, 2685–2700.
51. Merkwirth, C., Martinelli, P., Korwitz, A., Morbin, M., Bronneke, H.S., Jordan, S.D., Rugarli, E.I. and Langer, T. (2012) Loss of prohibitin membrane scaffolds impairs mitochondrial architecture and leads to tau hyperphosphorylation and neurodegeneration. *PLoS Genet*, **8**, e1003021.
52. Giannakopoulos, P., Herrmann, F.R., Bussiere, T., Bouras, C., Kovari, E., Perl, D.P., Morrison, J.H., Gold, G. and Hof, P.R. (2003) Tangle and neuron numbers, but not amyloid load, predict cognitive status in Alzheimer's disease. *Neurology*, **60**, 1495–1500.
53. Nagy, Z., Esiri, M.M., Jobst, K.A., Morris, J.H., King, E.M., McDonald, B., Litchfield, S., Smith, A., Barnetson, L. and Smith, A.D. (1995) Relative roles of plaques and tangles in the dementia of Alzheimer's disease: correlations using three sets of neuropathological criteria. *Dementia*, **6**, 21–31.
54. Mocanu, M.M., Nissen, A., Eckermann, K., Khlistunova, I., Biernat, J., Drexler, D., Petrova, O., Schonig, K., Bujard, H., Mandelkow, E. *et al.* (2008) The potential for beta-structure in the repeat domain of tau protein determines aggregation, synaptic decay, neuronal loss, and coassembly with endogenous Tau in inducible mouse models of tauopathy. *J. Neurosci.*, **28**, 737–748.
55. Van der Jeugd, A., Hochgrafe, K., Ahmed, T., Decker, J.M., Sydow, A., Hofmann, A., Wu, D., Messing, L., Balschun, D., D'Hooge, R. *et al.* (2012) Cognitive defects are reversible in inducible mice expressing pro-aggregant full-length human Tau. *Acta Neuropathol.*, **123**, 787–805.
56. Duyckaerts, C., Potier, M.C. and Delatour, B. (2008) Alzheimer disease models and human neuropathology: similarities and differences. *Acta Neuropathol.*, **115**, 5–38.
57. Distl, R., Treiber-Held, S., Albert, F., Meske, V., Harzer, K. and Ohm, T.G. (2003) Cholesterol storage and tau pathology in Niemann-Pick type C disease in the brain. *J. Pathol.*, **200**, 104–111.
58. Auer, I.A., Schmidt, M.L., Lee, V.M., Curry, B., Suzuki, K., Shin, R.W., Pentchev, P.G., Carstea, E.D. and Trojanowski, J.Q. (1995) Paired helical filament tau (PHFtau) in Niemann-Pick type C disease is similar to PHFtau in Alzheimer's disease. *Acta Neuropathol.*, **90**, 547–551.
59. Bu, B., Li, J., Davies, P. and Vincent, I. (2002) Deregulation of cdk5, hyperphosphorylation, and cytoskeletal pathology in the Niemann-Pick type C murine model. *J. Neurosci.*, **22**, 6515–6525.
60. Liu, B., Turley, S.D., Burns, D.K., Miller, A.M., Repa, J.J. and Dietschy, J.M. (2009) Reversal of defective lysosomal transport in NPC disease ameliorates liver dysfunction and neurodegeneration in the npc1-/- mouse. *Proc. Natl Acad. Sci. USA*, **106**, 2377–2382.
61. Davidson, C.D., Ali, N.F., Micsenyi, M.C., Stephney, G., Renault, S., Dobrenis, K., Ory, D.S., Vanier, M.T. and Walkley, S.U. (2009) Chronic cyclodextrin treatment of murine Niemann-Pick C disease ameliorates neuronal cholesterol and glycosphingolipid storage and disease progression. *PLoS One*, **4**, e6951.
62. Kowall, N.W. and Kosik, K.S. (1987) Axonal disruption and aberrant localization of tau protein characterize the neuropil pathology of Alzheimer's disease. *Ann. Neurol.*, **22**, 639–643.
63. Delacourte, A., Flament, S., Dibe, E.M., Hublau, P., Sablonniere, B., Hemon, B., Sherrer, V. and Defossez, A. (1990) Pathological proteins Tau 64 and 69 are specifically expressed in the somatodendritic domain of the degenerating cortical neurons during Alzheimer's disease. Demonstration with a panel of antibodies against Tau proteins. *Acta Neuropathol.*, **80**, 111–117.
64. Cowan, C.M., Quraishe, S. and Mudher, A. (2012) What is the pathological significance of tau oligomers? *Biochem. Soc. Trans.*, **40**, 693–697.
65. Bolmont, T., Clavaguera, F., Meyer-Luehmann, M., Herzig, M.C., Radde, R., Staufenbiel, M., Lewis, J., Hutton, M., Tolnay, M. and Jucker, M. (2007) Induction of tau pathology by intracerebral infusion of amyloid-beta -containing brain extract and by amyloid-beta deposition in APP x Tau transgenic mice. *Am. J. Pathol.*, **171**, 2012–2020.
66. Zempel, H., Thies, E., Mandelkow, E. and Mandelkow, E.M. (2010) Abeta oligomers cause localized Ca(2+) elevation, missorting of endogenous Tau into dendrites, Tau phosphorylation, and destruction of microtubules and spines. *J. Neurosci.*, **30**, 11938–11950.
67. Hernandez, P., Lee, G., Sjoberg, M. and Maccioni, R.B. (2009) Tau phosphorylation by cdk5 and Fyn in response to amyloid peptide Abeta (25–35): involvement of lipid rafts. *J. Alzheimers Dis.*, **16**, 149–156.
68. Schenck, A., Goto-Silva, L., Collinet, C., Rhinn, M., Giner, A., Habermann, B., Brand, M. and Zerial, M. (2008) The endosomal protein Appl1 mediates

Akt substrate specificity and cell survival in vertebrate development. *Cell*, **133**, 486–497.
69. Garcia-Ruiz, C., Mari, M., Colell, A., Morales, A., Caballero, F., Montero, J., Terrones, O., Basanez, G. and Fernandez-Checa, J.C. (2009) Mitochondrial cholesterol in health and disease. *Histol. Histopathol.*, **24**, 117–132.
70. Garcia-Ruiz, C., Morales, A. and Fernandez-Checa, J.C. (2012) Statins and protein prenylation in cancer cell biology and therapy. *Anticancer Agents Med. Chem.*, **12**, 303–315.
71. Eckert, G.P., Hooff, G.P., Strandjord, D.M., Igbavboa, U., Volmer, D.A., Muller, W.E. and Wood, W.G. (2009) Regulation of the brain isoprenoids farnesyl- and geranylgeranylpyrophosphate is altered in male Alzheimer patients. *Neurobiol. Dis.*, **35**, 251–257.
72. Hamano, T., Yen, S.H., Gendron, T., Ko, L.W. and Kuriyama, M. (2012) Pitavastatin decreases tau levels via the inactivation of Rho/ROCK. *Neurobiol. Aging*, **33**, 2306–2320.
73. Boimel, M., Grigoriadis, N., Lourbopoulos, A., Touloumi, O., Rosenmann, D., Abramsky, O. and Rosenmann, H. (2009) Statins reduce the neurofibrillary tangle burden in a mouse model of tauopathy. *J. Neuropathol. Exp. Neurol.*, **68**, 314–325.
74. Shankar, G.M., Li, S., Mehta, T.H., Garcia-Munoz, A., Shepardson, N.E., Smith, I., Brett, F.M., Farrell, M.A., Rowan, M.J., Lemere, C.A. *et al.* (2008) Amyloid-beta protein dimers isolated directly from Alzheimer's brains impair synaptic plasticity and memory. *Nat. Med.*, **14**, 837–842.
75. Braak, H. and Braak, E. (1991) Neuropathological staging of Alzheimer-related changes. *Acta Neuropathol.*, **82**, 239–259.
76. Juottonen, K., Laakso, M.P., Insausti, R., Lehtovirta, M., Pitkanen, A., Partanen, K. and Soininen, H. (1998) Volumes of the entorhinal and perirhinal cortices in Alzheimer's disease. *Neurobiol. Aging*, **19**, 15–22.
77. Delacourte, A., David, J.P., Sergeant, N., Buee, L., Wattez, A., Vermersch, P., Ghozali, F., Fallet-Bianco, C., Pasquier, F., Lebert, F. *et al.* (1999) The biochemical pathway of neurofibrillary degeneration in aging and Alzheimer's disease. *Neurology*, **52**, 1158–1165.
78. Clausen, A., Xu, X., Bi, X. and Baudry, M. (2012) Effects of the superoxide dismutase/catalase mimetic EUK-207 in a mouse model of Alzheimer's disease: protection against and interruption of progression of amyloid and tau pathology and cognitive decline. *J. Alzheimers Dis.*, **30**, 183–208.
79. McManus, M.J., Murphy, M.P. and Franklin, J.L. (2011) The mitochondria-targeted antioxidant MitoQ prevents loss of spatial memory retention and early neuropathology in a transgenic mouse model of Alzheimer's disease. *J. Neurosci.*, **31**, 15703–15715.
80. von Montfort, C., Matias, N., Fernandez, A., Fucho, R., Conde de la Rosa, L., Martinez-Chantar, M.L., Mato, J.M., Machida, K., Tsukamoto, H., Murphy, M.P. *et al.* (2012) Mitochondrial GSH determines the toxic or therapeutic potential of superoxide scavenging in steatohepatitis. *J. Hepatol.*, **57**, 852–859.
81. Tietze, F. (1969) Enzymic method for quantitative determination of nanogram amounts of total and oxidized glutathione: applications to mammalian blood and other tissues. *Anal. Biochem.*, **27**, 502–522.
82. Duncan, I.W., Culbreth, P.H. and Burtis, C.A. (1979) Determination of free, total, and esterified cholesterol by high-performance liquid chromatography. *J. Chromatogr.*, **162**, 281–292.
83. Greenberg, S.G. and Davies, P. (1990) A preparation of Alzheimer paired helical filaments that displays distinct tau proteins by polyacrylamide gel electrophoresis. *Proc. Natl Acad. Sci. USA*, **87**, 5827–5831.
84. Schmued, L.C., Albertson, C. and Slikker, W. Jr (1997) Fluoro-Jade: a novel fluorochrome for the sensitive and reliable histochemical localization of neuronal degeneration. *Brain Res.*, **751**, 37–46.
85. Morris, R. (1984) Developments of a water-maze procedure for studying spatial learning in the rat. *J. Neurosci. Methods*, **11**, 47–60.
86. Bevins, R.A. and Besheer, J. (2006) Object recognition in rats and mice: a one-trial non-matching-to-sample learning task to study 'recognition memory'. *Nat. Protoc.*, **1**, 1306–1311.